J. Phys. Chem. Solids Vol. 48, No. 11, pp. 985–1005, 1987
Printed in Great Britain.

0022-3697/87 $3.00 + 0.00

CRACK TIP PLASTICITY IN DYNAMIC FRACTURE

P. A. MATAGA,†
Division of Applied Sciences, Harvard University, Cambridge, Massachusetts 02138, U.S.A.

L. B. FREUND
Division of Engineering, Brown University, Providence, Rhode Island 02912, U.S.A.

J. W. HUTCHINSON
Division of Applied Sciences, Harvard University, Cambridge, Massachusetts 02138, U.S.A.

Abstract—The mechanics of crack tip plasticity in dynamic crack growth is considered as it influences two modes of dynamic fracture—cleavage and micro-void nucleation, growth and coalescence. The subject is approached using both the continuum theory of visco-plasticity and dislocation dynamics. The viewpoint underlying each approach is that the crack is traveling through material with a relatively high density of pre-existing mobile dislocations. Analysis is directed at discovering the role played by the associated rate-dependent plasticity in establishing conditions for dynamic crack propagation. The theory is far from complete, but the contents of the paper should serve to aid understanding of basic material fracture phenomena, such as cleavability and the ductile–brittle transition, as well as provide a background for the engineering theory of dynamic fracture.

Keywords: Dynamic fracture, plasticity, cleavability, ductile–brittle transition.

1. INTRODUCTION

This paper focuses on conditions for rapid crack propagation in metals using both the continuum theory of plasticity and a dislocation theory. The underlying premise of the paper is that a dislocation source distribution and/or a mobile dislocation density exists in the material prior to the cracking event such that plastic dissipation in a zone around the tip of the crack plays an essential role in setting conditions for propagation or arrest. This premise is of necessity in effect when a crack advances by the mechanism of micro-void nucleation, growth and coalescence. In this mode of growth, relatively large strains must occur in the fracture process zone, which is typically many microns in extent, and substantial plasticity occurs in a zone surrounding the fracture process zone as well. The premise also often holds for cleavage cracking of single crystal and polycrystalline metals even though the fracture process itself is not necessarily accompanied by extensive plastic deformation.

This paper does not address the "intrinsic cleavability" of a given metal. Investigations of intrinsic cleavability of a single crystal of a given material (e.g. [1–3]) generally assume that background dislocations in the vicinity of the crack tip are absent and consider a competition between dislocation emission from the tip and the atomic separation process. Given that a material is intrinsically cleavable, whether or not a crack advances by cleavage in a typical test situation seems to be greatly influenced by the interaction of the crack tip with pre-existing background dislocations. It is not even known, for example, whether a phenomenon as dramatic and basic as the ductile–brittle transition observed in many metals represents a loss in intrinsic cleavability or whether it is primarily due to crack tip interaction with the background dislocation field. Recent discussion has called attention to the apparent limitations of various measures of intrinsic cleavability in classifying observed cleavability of a wide range of materials. A simple model has been used in Ref. [4] to estimate the effect of pre-existing dislocation density on the ductile–brittle transition; critical densities in the observable range are predicted.

A continuum theory of crack tip plasticity does not distinguish between the motion of dislocations emitted from the tip and those pre-existing in the interior of the solid or nucleated from internal sources. However, it is assumed that the scale of the inelastic deformation, the plastic zone size, is very large compared to the dislocation spacing and the travel distance of individual dislocations. Our objective is to discuss quantitative estimates of the stress field and plastic dissipation in the region surrounding the crack tip. We will not attempt to characterize details of the fracture process itself. The extent of the fracture process zone when the micro-void mechanism operates is some multiple (typically, from 2 to 20) times the spacing of the void nucleating particles. Because the growth and coalescence process generally requires relatively large plastic strains, crack advance by this mechanism is innately accompanied by substantial plastic deformation, both in the fracture process zone and without, as has already been remarked. By

† Currently at Materials Program, College of Engineering, University of California, Santa Barbara, CA 93106, U.S.A.

contrast, cleavage is not necessarily accompanied by plastic deformation and in fact the essence of cleavage in many metals seems to be tied to the ability of the crack to outrun most of the plastic deformation which would otherwise accumulate if it were advancing quasi-statically.

Stroh's [5] early discussion of the micro-mechanics of cleavage fracture gives a remarkably clear picture of some of the qualitative aspects of the process. For many metals, cleavage appears to be an inherently dynamic process in which a crack somehow gets started running at high speed. The rate-dependence of plastic flow enables the crack to outrun most of the plastic deformation. The mechanism of crack advance by void growth was not appreciated at the time Stroh wrote his article. It is of historical interest to read of Stroh's insightful groping for a mechanism other than cleavage to explain phenomena which clearly did not fit into his view of cleavage.

The outline of the present paper is as follows. Aspects of high strain rate plasticity are discussed in section 2. Some of the most relevant results from elasto-dynamic fracture mechanics are summarized in section 3 along with an asymptotic result for the plastic dissipation at a steady running crack tip when the dissipation is not too large. The most complete results available for elucidating the role of crack tip plasticity over the full range of crack velocities, from quasi-static to high speed, are for the anti-plane shear problem (mode III) [6], and these results will be given in section 4. Plane strain, mode I, high speed crack growth is discussed in section 5 from the vantage point of continuum plasticity theory following the treatment in Refs [6–8]. The initial steps in a parallel treatment which accounts for the motion of individual dislocations is given in section 6, permitting the results of the continuum theory to be reinterpreted in dislocation terms. Throughout the paper, application of the theory to establish conditions for crack propagation and arrest will be discussed with a strong distinction drawn between conditions appropriate for the two fracture mechanisms, cleavage and the micro-void process. In addition, implications of the theory are discussed related to a number of central issues such as the ductile–brittle transition, suppression of cleavage, velocity–toughness relations and crack arrest.

2. HIGH STRAIN RATE PLASTICITY

The strain rates experienced by material elements close enough to the crack tip to undergo plastic deformation are generally very large for typical crack velocities, usually well above $10^3\,s^{-1}$ and as large as $10^6\,s^{-1}$ or more. Although data on metal deformation at strain rates as high as $10^6\,s^{-1}$ is rare, it is well established that many metals display sharply increasing resistance to plastic flow at strain rates above, typically, $10^3\,s^{-1}$. The effect of this elevation in flow resistance has very different consequences for cleavage and for fracture by the micro-void mechanism, as will be seen.

A running crack tip subjects nearby material elements to a very brief stress pulse. This pulse results in relatively small amounts of plastic strain in the case of cleavage cracking and relatively large plastic strain for a crack advancing by the micro-void mechanism. As discussed below, high strain rate data is not usually gathered under conditions which model a brief stress pulse resulting in small plastic strains. Consequently, the constitutive law for material behavior in the inelastic zone of a cleavage crack can only be inferred from data taken under other high strain rate histories.

Most high strain rate tests are conducted in the manner indicated in Fig. 1(a). Specimens are tested under a sequence of strain rates, each specimen being subject to a nominally homogeneous strain and constant strain rate over the entire test history. A series of stress–strain curves, plotted as shear stress τ vs plastic shear strain γ^p in Fig. 1(a), are generated, each associated with a particular strain rate. This data is then cross-plotted as in Fig. 1(b) as τ vs $\dot{\gamma}^p$ at a given level of plastic strain. The relation of τ to $\dot{\gamma}^p$ reflects the visco-plastic nature of the response. Most data of this type (e.g. [9–12]) display a fairly dramatic increase in flow resistance at strain rates above a transition rate $\dot{\gamma}_t$ about $10^3\,s^{-1}$ or $10^4\,s^{-1}$. The transi-

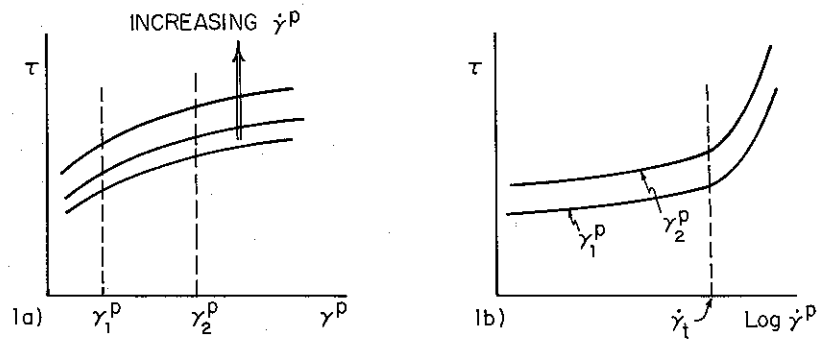

Fig. 1. High strain rate testing. (a) Data as collected, in the form of relation between shear stress and plastic shear strain for nominally constant strain rates; (b) data cross-plotted as relation between shear stress and plastic shear strain rate for given levels of plastic strain.

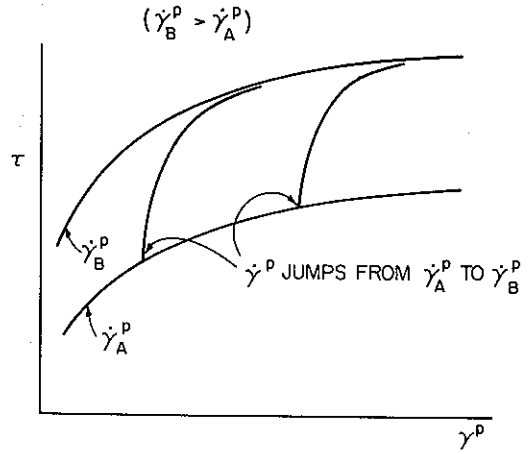

Fig. 2. Transient strain histories produced by high strain rate pulse acting on material initially deformed at low strain rate.

tion is usually attributed to dislocation velocities being pushed into the phonon drag regime [13], but the particular mechanism is not important for present purposes. Simple dislocation models, which neglect the multiplication of mobile dislocations, indicate that τ increases in linear proportion to increases in $\dot{\gamma}^p$ in this regime. Some data of the type depicted in Fig. 1(b) are in approximate accord with the linear dependence, at least over a limited range of strain rates above $\dot{\gamma}_t$ [12].

Recently it has been argued [11] that the state of the material following a given plastic strain depends strongly on the strain rate which occurred over the strain history. Such a dependence is also evident in data taken under transient histories where a specimen experiences a high strain rate pulse (but with $\dot{\gamma}^p < \dot{\gamma}_t$) following straining at a low strain rate [12]. Figure 2 depicts the nature of such transient histories. Once the high strain rate pulse starts, the stress increases rapidly and approaches the stress associated with the history in which the strain rate is the high value from the start of straining. It is data of this type which should be most relevant to the brief stress pulse associated with a running crack, particularly for cleavage cracking where relatively small plastic strain increments are induced. One would expect the pre-cracked material to have a dislocation structure which arose as the result of one or more low strain rate processing steps, and it is on this pre-existing structure that the stress pulse acts.

The idealized mechanical models of material behavior used to obtain the results described below are visco-plastic in character such that the plastic strain rate during a brief pulse is taken to be given by

$$\dot{\gamma}^p = F(\tau), \tag{2.1}$$

with any explicit dependence on strain omitted due to its seemingly secondary significance. For cleavage cracking, strain hardening should be of secondary importance since the increments in plastic strain are small. For a crack advancing at high speed by the micro-void process, strain hardening is likely to be more important, but it will not be accounted for here. In either case, when $F(\tau)$ is identified with data cross-plotted in the manner of Fig. 1(b), the strain level γ^p associated with the cross-plot should be representative of that occurring in the plastic zone.

Specifically, we will consider two visco-plastic idealizations. The simplest is that in Fig. 3(a) where the material is elastic-perfectly plastic with $\tau = \tau_t$ for $\dot{\gamma}^p \le \dot{\gamma}_t$ and

$$\dot{\gamma}^p = \dot{\gamma}_t + \dot{\gamma}_0(\tau - \tau_t)/\mu \quad \text{for} \quad \tau > \tau_t, \tag{2.2}$$

where μ is the elastic shear modulus. For the relation displayed in Fig. 3(b), the material has a relatively weak stress dependence below the transtion stress τ_t, such as that suggested in Ref. [13] and used in Refs [7, 8]. Above the transition stress, the material will be characterized by either eqn (2.2) or the slightly more elaborate representation

$$\dot{\gamma}^p = \dot{\gamma}_t + \dot{\gamma}_A\left(\frac{\tau - \tau_t}{\tau_t}\right) + \dot{\gamma}_B\left(\frac{\tau - \tau_t}{\tau_t}\right)^n \quad (\tau > \tau_t). \tag{2.3}$$

This latter representation is motivated by a suggestion in Ref. [10] that the dependence of plastic strain rate on stress may approach a power law relation at very high stresses, where the stress ex-

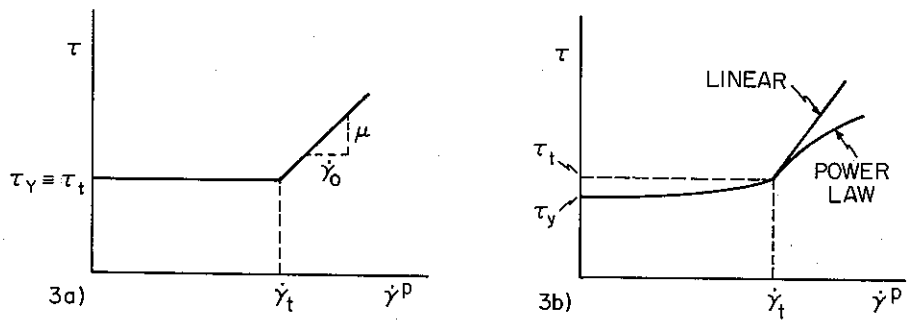

Fig. 3. Visco-plastic idealizations of material behavior. (a) Elastic/perfectly-plastic at low strain rate, linear stress dependence at high strain rate; (b) weak stress dependence at low strain rate, linear or power law stress dependence at high strain rate.

ponent may be between 2 and 3. Our analysis can embrace eqn (2.3) with no extra complication and thus eqn (2.3) will also be considered. However, most of the discussion which follows will center on eqn (2.2).

The multi-axial form of the constitutive law is based on the Mises stress invariant in the usual way. With σ_{ij} as the stress, s_{ij} as the stress deviator, and $\tau = (s_{ij}s_{ij}/2)^{1/2}$ as the effective shear stress, the plastic strain rate is

$$\dot{\varepsilon}^p_{ij} = F(\tau)s_{ij}/(2\tau). \tag{2.4}$$

The total strain rate is $\dot{\varepsilon}_{ij} = \dot{\varepsilon}^e_{ij} + \dot{\varepsilon}^p_{ij}$ where the elastic part is given by

$$\dot{\varepsilon}^e_{ij} = \frac{1}{E}[(1+\nu)\dot{\sigma}_{ij} - \nu\dot{\sigma}_{kk}\delta_{ij}], \tag{2.5}$$

where E is Young's modulus and ν is Poisson's ratio.

The general visco-plastic relation (2.4) continues to apply under conditions of decreasing effective shear stress; the material description then implies a transition to an elastic unloading regime when τ falls below the level at which $F(\tau) = 0$.

3. ELASTIC CRACK PROPAGATION AND STEADY-STATE GROWTH IN SMALL SCALE YIELDING

3.1. *Elasto-dynamic results*

The elasto-dynamic stress fields at the tip of a crack lying on the x_1-axis and advancing with velocity v in the x_1-direction in a linear, isotropic elastic solid are of the form

$$\sigma_{ij} = \frac{K}{\sqrt{2\pi r}}\Sigma_{ij}(\theta, m), \tag{3.1}$$

where r and θ are planar polar coordinates centered at the tip. The normalized velocity m is defined by

$$m = v/c_r \quad \text{(mode I)},$$
$$= v/c_s \quad \text{(mode III)}, \tag{3.2}$$

where c_r is the Rayleigh wave speed and c_s is the shear wave speed. The functions $\Sigma_{ij}(\theta, m)$ are universal for a given mode of loading, and K is the associated *dynamic* stress intensity factor. In mode I the normalization $\Sigma_{22} = 1$ is used on the line ahead of the tip, while $\Sigma_{23} = 1$ is used in mode III. In mode III

$$\Sigma_{23} + i\alpha_s\Sigma_{13} = (\cos\theta - i\alpha_s\sin\theta)^{-1/2}, \tag{3.3}$$

where $\alpha_s = (1-m^2)^{1/2}$ and $i = \sqrt{-1}$. The corresponding formulae in mode I are slightly more complicated; they can be found in Refs [7, 14, 15].

The fundamental relation between the dynamic elastic energy release rate G (the energy "loss" out the tip per unit of crack extension per unit length of crack front) and the dynamic stress intensity factor is

$$G = f(m)(1-\nu^2)K^2/E \quad \text{(plane strain, mode I)}, \tag{3.4}$$

$$G = (1-m^2)^{-1/2}K^2/(2\mu) \quad \text{(mode III)}, \tag{3.5}$$

where $f(0) = 1$ and $f(m)$ has a dependence on m much like $(1-m^2)^{-1/2}$, together with a very weak dependence on ν [14].

The quantities K or G characterize the near-tip field of the running crack in any elastic problem. The solution to an elasto-dynamic problem provides the history of K or G as a function of the history of the crack tip position and loading. Few closed form solutions are available which provide the time history of K or G, but one example discussed in Ref. [14] nicely illustrates the way K or G depends on crack velocity and applied load. Imagine a crack running into a block of pre-stressed material. Let K_S denote the static stress intensity factor of a stationary crack in the pre-stressed block whose length coincides momentarily with that of the dynamic crack, and let $G_S = (1-\nu^2)K_S^2/E$ be the corresponding quasi-static energy release rate. As long as there are no wave reflections from the outer surfaces of the block or from the other end of the crack back onto the tip, then the dynamic energy release rate of the running crack is given by G_S times a function of m. To a good approximation

$$G \cong (1-m)G_S, \tag{3.6}$$

reflecting the tendency for the energy release at the tip to be reduced at high velocities due to inertial shielding. This simple result will be useful in interpreting some of the theoretical predictions later in the paper.

3.2. *Steady-state, small scale yielding*

In this paper we will discuss solutions to several steady-state crack problems where the active plastic zone is small compared to all geometric length scales, including the crack length itself. In the small scale yielding problem (see Fig. 4) one focuses on behavior near the crack tip in the plastic zone by posing an asymptotic problem in which the remote, or outer, solution is the elasto-dynamic field [eqn (3.1)] characterized by K or, equivalently, by G. The plastic zone size scales as $(K/\tau_Y)^2$ or $\mu G/\tau_Y^2$ where τ_Y is an appropriate yield stress. As indicated in Fig. 4, the outer part of the active plastic zone is generally characterized by plastic strain rates below the transition $\dot{\gamma}_t$, while the inner region surrounding the tip is the high strain rate regime. A wake of residual plastic strains is left behind the active plastic zone advancing with the tip. In the steady-state problem an observer moving with the tip sees an unchanging field. The time derivative of any Cartesian component of any field quantity associated with a material point is

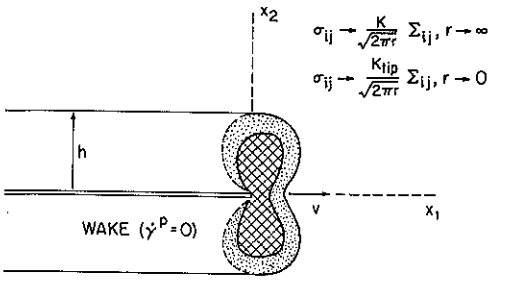

Fig. 4. Dynamic steady-state, small scale yielding crack propagation.

related to the x_1-gradient by

$$(\dot{}) = -v\frac{\partial}{\partial x_1}(). \tag{3.7}$$

The studies reported below are carried out in plane strain or anti-plane shear within the context of the small strain theory of plasticity so that linearized equilibrium and strain–displacement relations are used.

An important feature of each of the problems for propagation in rate-dependent materials discussed in this paper is that the elastic strain rates become large compared to the plastic strain rates as $r \to 0$. This fact, which requires the stress exponent n in eqn (2.3) to be less than 3, is easily established using arguments similar to those in Refs [16–19]. An important consequence of this fact is that the asymptotic near-tip stress fields within the high strain rate zone have precisely the same form as in the elastic problem, except that the amplitude will be reduced below K by the plasticity. That is,

$$\sigma_{ij} = \frac{K_{tip}}{\sqrt{2\pi r}} \Sigma_{ij}(\theta, m) \quad \text{as} \quad r \to 0 \tag{3.8}$$

and the crack tip energy release rate is given by

$$G_{tip} = f(m)(1-\nu^2)K_{tip}^2/E \quad \text{(mode I)}, \tag{3.9}$$

$$G_{tip} = (1-m^2)^{-1/2}K_{tip}^2/(2\mu) \quad \text{(mode III)}. \tag{3.10}$$

The main result from each of the small scale yielding problems is the relation between G_{tip} and G as influenced by the parameters of the visco-plastic material model and the crack velocity. The basic steady-state energy balance is [7]

$$G_{tip} = G = \frac{1}{v}\int_A \sigma_{ij}\dot{\varepsilon}_{ij}^p \, dA - \int_{-h}^{h} U_e \, dx_2, \tag{3.11}$$

where the area integral extends over the active plastic zone and U_e denotes the residual elastic strain energy density in the remote wake. Within the context of the continuum theory, G_{tip} must be regarded as the energy rate available for the fracture processes deep within the plastic zone. In other words, the continuum theory discussed here accounts for the plastic dissipation in the plastic zone, but not that associated with the fracture process itself; the fracture process consumes the energy flowing out the tip as given by G_{tip} in the continuum solution. The continuum approach is then meaningful in application to dynamic crack growth to the extent that the fracture process can be decoupled energetically from the plastic dissipation in the plastic zone.

An asymptotic expression for the plastic dissipation term in eqn (3.11) was derived in Ref. [7] which is valid under conditions, to be discussed in detail in what follows, when the plastic dissipation is not too large compared to G. Moreover, under these conditions the contribution of the residual elastic energy left in the wake is extremely small and unimportant in the energy balance of eqn (3.11). When the crack runs rapidly with relatively little plastic dissipation, nearly all the plastic dissipation which does occur is associated with plastic strain rates in the high strain rate regime ($\dot{\gamma}^p > \dot{\gamma}_t$), and these plastic strain rates can be calculated using the near tip stress field [eqn (3.8)]. The calculation for plane strain gives (see Ref. [7] for details)

$$\frac{1}{v}\int_A \sigma_{ij}\dot{\varepsilon}_{ij}^p = \frac{2}{\pi^2}\frac{B(m)\mu^2}{[(1-\nu)f(m)]^2}\frac{G_{tip}^2}{v} \times \int_{\tau_t}^{\infty} F(\tau)\tau^{-4}\,d\tau, \tag{3.12}$$

where

$$B(m) = \int_{-\pi}^{\pi} [\tfrac{1}{2}\Sigma'_{ij}(\theta)\,\Sigma'_{ij}(\theta)]^2 \, d\theta, \tag{3.13}$$

and

$$\Sigma'_{ij} = \Sigma_{ij} - \tfrac{1}{3}\Sigma_{kk}\delta_{ij}.$$

For the linear relation (2.2),

$$\int_{\tau_t}^{\infty} F(\tau)\tau^{-4}\,d\tau = \tau_t^{-3}\left[\frac{1}{3}\dot{\gamma}_t + \frac{1}{6}\frac{\tau_t}{\mu}\dot{\gamma}_0\right] \equiv \tau_t^{-3}\tilde{\dot{\gamma}}, \tag{3.14}$$

while for the more elaborate representation (2.3),

$$\int_{\tau_t}^{\infty} F(\tau)\tau^{-4}\,d\tau = \tau_t^{-3}\left[\frac{1}{3}\dot{\gamma}_t + \frac{1}{6}\dot{\gamma}_A + c(n)\dot{\gamma}_B\right] \equiv \tau_t^{-3}\tilde{\dot{\gamma}}, \tag{3.15}$$

where for $n < 3$

$$c(n) = \int_1^{\infty} \xi^{-4}(\xi-1)^n \, d\xi = \frac{\pi}{6}\frac{n(n-1)(n-2)}{\sin n\pi}. \tag{3.16}$$

Values of $c(n)$ are listed in Table 1.

Table 1. Selected values of $c(n)$

n	1	$\frac{3}{2}$	2	$\frac{5}{2}$	3
$c(n)$	$\frac{1}{6}$	$\frac{\pi}{16}$	$\frac{1}{3}$	$\frac{5\pi}{16}$	∞

With $\dot{\gamma}$ denoting the collection of strain rate-like terms defined in eqns (3.14) or (3.15), depending on the representation used, the asymptotic energy balance (3.11) can be written as

$$G_{tip} = G - H(m)\left(\frac{\dot{\gamma}\mu^2}{\tau_i^3 v}\right)G_{tip}^2, \qquad (3.17)$$

where

$$H(m) = \frac{2}{\pi^2}\frac{B(m)}{[(1-\nu)f(m)]^2}. \qquad (3.18)$$

This reduces to the equation in Ref. [7] for the case of the linear representation for the high strain rate regime; however, the terms in the plastic dissipation have been regrouped here. In particular, the effect of inertia comes in exclusively through $H(m)$ which is presented in Fig. 5 and Table 2 for $\nu = 0.29$. For m less than about 0.3 inertia has almost no effect on the energy balance [eqn (3.17)]. In the limit $m \to 0$, $H = 0.0810$ for $\nu = 0.29$, and the relation becomes

$$G_{tip} = G - 0.0810\left(\frac{\dot{\gamma}\mu^2}{\tau_i^3 v}\right)G_{tip}^2, \qquad (3.19)$$

which is precisely the result one would obtain from an analysis which neglected inertia from the start.

In mode III, eqn (3.12) still holds but with $(1-\nu)f(m)$ replaced by $(1-m^2)^{-1/2}$ where, now, $m = v/c_s$. The integral (3.13) for $B(m)$ can be evaluated analytically. The resulting energy balance is again eqn (3.17) where now

$$H(m) = \frac{4}{\pi}\frac{1-m^2+3m^4/8}{(1-m^2)^{3/2}} \quad \text{(mode III)}. \qquad (3.20)$$

The asymptotic equation (3.17) for G_{tip} in terms of G will be compared with accurate numerical results in the next section. It will be seen that a slight modification of this equation leads to a result with improved accuracy at relatively large plastic dissipation.

4. STEADY-STATE, SMALL SCALE YIELDING CRACK GROWTH IN MODE III

Mode III (anti-plane shear) crack problems have a long and useful history in fracture mechanics as mathematical models of their counterparts in plane strain or plane stress which are generally more difficult to analyze. In dynamic crack propagation this utility persists even though the cleavage process itself is not a mode III phenomenon. The mode III problem provides relationships between variables such as G_{tip} and G which are similar to those for the plane problems. At the present time, the most complete picture of crack growth is that for mode III.

4.1. *Quasi-static and dynamic growth in rate-insensitive, perfectly-plastic solids*

With τ_Y as the yield stress in shear of an isotropic, elastic/perfectly-plastic solid, the yield condition according to the Mises criterion or the maximum shear stress criterion is $\tau_1^2 + \tau_2^2 = \tau_Y^2$, where the notation for mode III is displayed in Fig. 6. We first give the *quasi-static* (i.e. inertia-free) result for the shear strain distribution on the line ahead of the crack ($\theta = 0$) within the plastic zone [20, 21]:

$$\gamma_2 = \gamma_Y[1 + \ln(R/x_1) + \tfrac{1}{2}\ln^2(R/x_1)], \qquad (4.1)$$

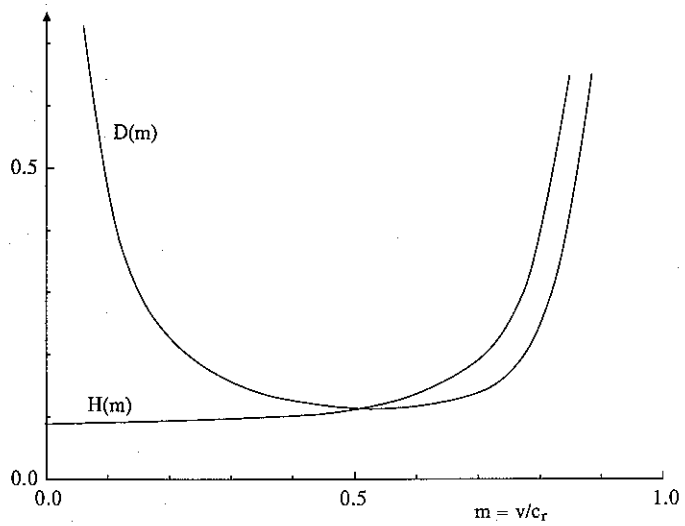

Fig. 5. $H(m)$ and $D(m)$ in plane strain, mode I ($\nu = 0.29$). The value of H at $m = 0$ is 0.081. The minimum value of D is 0.109 at $m = 0.55$. [D is defined below by eqn (5.6).]

Table 2. Selected values of $H(m)$ and $D(m)(\nu = 0.29)$

m	0	0.1	0.2	0.3	0.4	0.5	0.6	0.7	0.8	0.9
$H(m)$	0.081	0.081	0.083	0.086	0.092	0.102	0.123	0.175	0.345	1.484
$D(m)$	∞	0.441	0.224	0.155	0.124	0.110	0.111	0.135	0.233	0.892

where $\gamma_Y = \tau_Y/\mu$. The distance R the plastic zone extends ahead of the crack tip is *ca* 7% less than the corresponding distance for the stationary problem, i.e. 7% less than

$$R = (2/\pi)G\mu/\tau_Y^2. \tag{4.2}$$

The near-tip strain field in the steady-state quasi-static growth problem is significantly less singular than for the stationary problem, where $\gamma_2 = \gamma_Y R/x_1$ on the line ahead of the tip in the plastic zone. It is even less singular than that for the linear elastic problem at the same level of G. The energy release rate at the tip, G_{tip}, is identically zero, implying that all the energy released from the remote field G is consumed by plastic dissipation [21]. Consequently, within the context of the problem of a line crack in a rate-independent solid, it is not possible to accommodate a criterion for propagation based on a critical near-tip energy release rate. The dramatic reduction in the strain levels ahead of a growing crack compared to the stationary crack leads to the highly stable crack growth characteristics of cracks advancing by the micro-void mechanism in ductile metals [21, 22].

Some sense of the implications of the mode III model for crack growth under ductile void growth conditions can be had using the simple strain-based criterion [22] for continuing crack advance that the plastic strain a distance x_c ahead of the tip maintains a critical value, i.e.

$$\gamma_2^p = \gamma_c \quad \text{at} \quad x_1 = x_c. \tag{4.3}$$

Imposition of eqn (4.3) on the stationary solution for initiation of advance gives

$$R_{init}/x_c = 1 + \gamma_c/\gamma_Y, \tag{4.4}$$

while imposition of eqn (4.3) on the steady-state solution (4.1) gives

$$R_{ss}/x_c = \exp[(1 + 2\gamma_c/\gamma_Y)^{1/2} - 1]. \tag{4.5}$$

Thus, the ratio of the plastic zone size associated with steady-state growth to that associated with initiation is

$$R_{ss}/R_{init} = (1 + \gamma_c/\gamma_Y)^{-1} \exp[(1 + 2\gamma_c/\gamma_Y)^{1/2} - 1], \tag{4.6}$$

which becomes large when γ_c/γ_Y is large. Based on the ductile propagation criterion (4.3), resistance curves in the form of G vs crack advance Δa have been determined in Refs [21, 22]. These have the form shown on the left in Fig. 7 where steady-state conditions are approached after a crack advance of about, typically, 2 or 3 times R_{ss}.

The strain distribution ahead of the crack for the *dynamic, elastic/perfectly-plastic problem* in which inertia is included is more complicated that that for the quasi-static limit, but it has also been obtained in closed form [23]. Within the plastic zone it has the form

$$\gamma_2 = \gamma_Y f(m, R/x_1), \tag{4.7}$$

where $m = v/c_s$ and R is again the distance to the elastic/plastic boundary directly ahead of the tip. Equation (4.7) reduces to the quasi-static result (4.1) as $m \to 0$. The distance to the elastic/plastic boundary must be obtained by a numerical solution to the steady-state problem. An approximate expression for R obtained by fitting numerical results for $m \leq 0.6$ is [23]

$$R = (0.59 - 1.0m^2)(1 - m^2)^{1/2}(\mu G/\tau_Y^2). \tag{4.8}$$

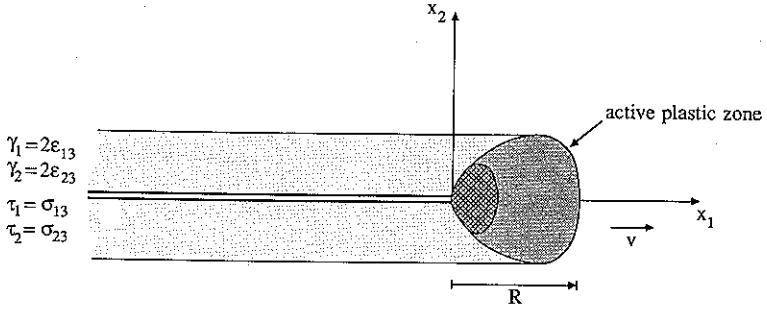

Fig. 6. Notation for mode III steady-state, small scale yielding crack propagation.

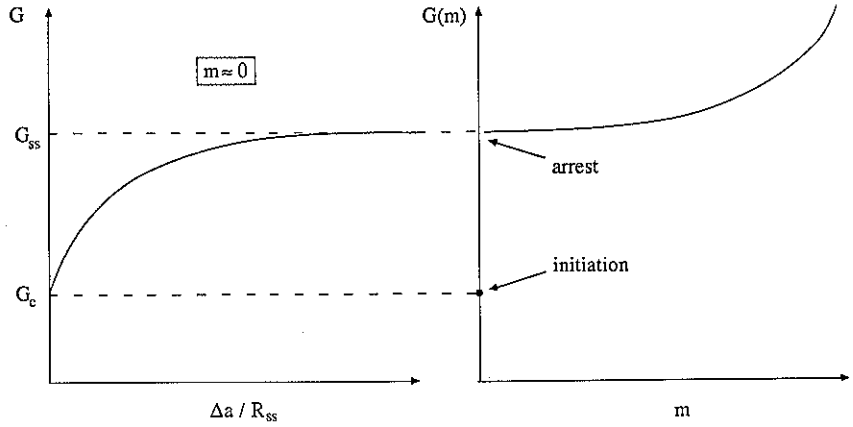

Fig. 7. Resistance curves for elastic/perfectly-plastic material for a strain-based propagation criterion such as eqn (4.3). On the left G is plotted against crack advance for transient quasistatic crack advance. On the right G is plotted against normalized crack speed for steady-state dynamic crack advance.

To see the effect of inertia on steady-state, ductile crack growth, the authors in Ref. [23] also imposed the criterion for crack advance eqn (4.3) on (4.7), to obtain

$$\gamma_c/\gamma_Y = f(m, R/x_c) - 1. \tag{4.9}$$

The dependence of G on m is obtained by eliminating R using eqn (4.8). Figure 8 displays the ratio of the value of G needed to drive the crack at velocity m from eqn (4.9) to the value of G needed to drive the crack quasi-statically from eqn (4.9) with $m = 0$. Alternatively, the quasi-static value can be obtained from eqns (4.2) and (4.5) as

$$G(m=0) = 1.69(x_c\tau_Y^2/\mu) \times \exp\{(1 + 2\gamma_c/\gamma_Y)^{1/2} - 1\}. \tag{4.10}$$

The ratio in Fig. 8 is independent of x_c. The more ductile the material (i.e. the larger is γ_c/γ_Y), the lower the crack velocity where inertial effects start to become important. For the rate-insensitive material advancing according to the simple *strain-based* growth criterion, the steady-state velocity increases monotonically with G.

Experimentally measured relations between the dynamic K or G and velocity under conditions of plane strain, mode I show the trends predicted by the mode III model when the material fractures by the micro-void mechanism. Figure 9 presents such data from Ref. [24] for a high strength steel (AISI 4340) which has a very low strain rate sensitivity and which did fracture by the micro-void mechanism. The data in Fig. 9 is plotted as K_{Ic}^d (which is just K in the notation of the present paper) as a function of velocity. The data is taken under conditions involving significant crack extension but not, of course, strictly steady-state. The data point associated with $v = 0$ is the crack arrest value for the running crack and *not* the initiation fracture toughness, K_{Ic}, of the material. The initiation toughness for this material is about 15% below the arrest value of K. This is to be expected since the arrest value of K or G for a running crack should be essentially the quasi-static, steady-state value, i.e. $G_a \cong G_{ss}$, assuming the crack is running into a slowly varying stress field. This value, in turn, should always exceed the value of K or G needed to initiate crack growth in a standard fracture toughness test of a material fracturing by the micro-void mechanism.

The relationship between the behavior of the crack under quasi-static advance starting from initiation and the nominally steady-state behavior of the running crack is shown schematically in Fig. 7. If the material has substantial tearing resistance with a quasi-static G value for steady-state growth, G_{ss}, many times the initiation value G_c, then the relation between G and m for the running crack will be correspondingly high, assuming of course that the micro-void mechanism does not give way to cleavage. The AISI 4340 steel, for which data was presented in

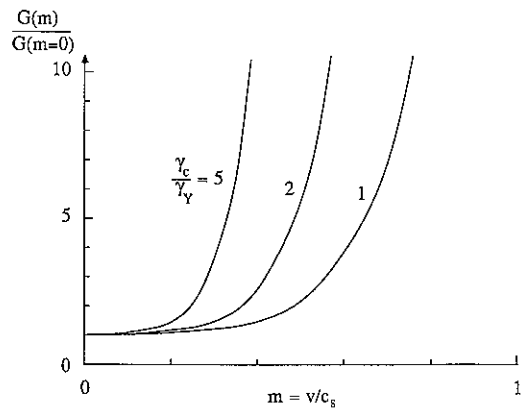

Fig. 8. Value of G needed to drive crack at normalized crack speed m in rate-independent elastic/plastic material compared to quasistatic value $G(m = 0)$, plotted for various γ_c/γ_Y.

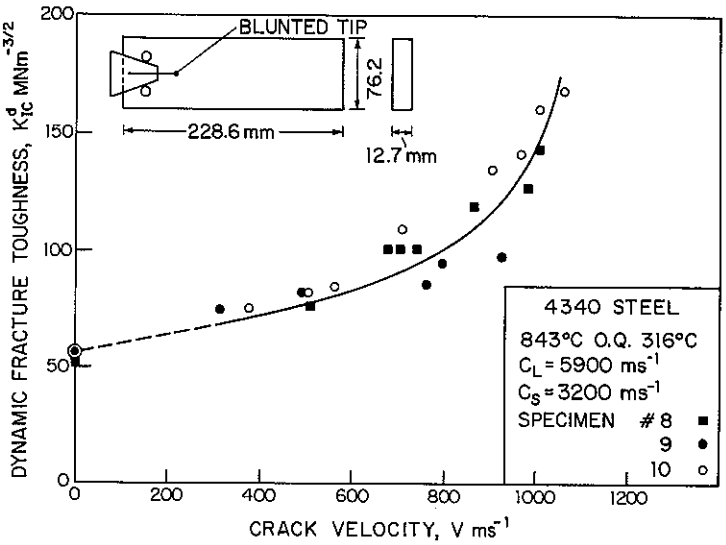

Fig. 9. Experimentally measured relation between dynamic stress intensity factor and crack speed for a high strength steel (reproduced from Ref. [24]).

Fig. 9, had only modest tearing resistance, and thus K_{Ia} did not exceed K_{Ic} by a large factor.

4.2. *Crack growth in rate-dependent solids*

The mode III results in this subsection are all based on the idealized visco-plastic shear stress–strain rate curve shown in Fig. 3(a). The response of the material is elastic/perfectly-plastic with $\tau = \tau_Y \equiv \tau_t$ for $\dot{\gamma}^p < \dot{\gamma}_t$ and with $\dot{\gamma}_p$ given by the linear representation (2.2) in the high strain rate regime for $\dot{\gamma}^p > \dot{\gamma}_t$ and $\tau > \tau_t$.

The solution to the small scale yielding, steady-state problem depends on three dimensionless combinations and these are conveniently chosen to be

$$m = \frac{v}{c_s}, \quad \zeta = \frac{\mu\dot{\gamma}_t}{\tau_t\dot{\gamma}_0} \quad \text{and} \quad Q = \frac{\mu\dot{\gamma}_0 G}{c_s\tau_t^2}. \tag{4.11}$$

Results for the distribution of plastic shear strain ahead of the tip and for G_{tip}/G [6] were obtained using a finite element scheme specially adapted to the steady-state problem along the lines of previous studies [8, 23, 25]. The numerical calculations were made for the following combination of parameters: $m = 0.03,\ 0.1,\ 0.3,\ 0.5,\ 0.8$; $\zeta = 0.01,\ 0.1$; with Q ranging from 0.01 to 100. For iron-based materials we have estimated ζ to be of the order of 10^{-2}. In the range of relatively small values of ζ considered here, the solution displays little dependence on this parameter. The Q parameter is strongly material dependent ranging from as small as 0.005 for cleavage micro-cracking of a single crystal of iron to more than 50 for crack propagation in a tough polycrystalline steel.

Some selected results for the distribution of γ_2^p ahead of the tip are shown in Fig. 10. The distributions in Fig. 10(a) are for several values of m with a common value of Q. The limiting curve for $m = 0$ coincides with the rate-independent, perfectly plastic distribution (4.1) because the portion of the plastic zone in which $\dot{\gamma}^p > \dot{\gamma}_t$ shrinks to zero as $m \to 0$. As m increases, the high strain rate regime ($\dot{\gamma}^p > \dot{\gamma}_t$) occupies a larger and larger fraction of the active plastic zone. If

$$\frac{v\tau_t^3}{\dot{\gamma}_t\mu^2 G} \equiv \frac{m}{\zeta Q} > \tfrac{1}{2} \text{ to } 2 \tag{4.12}$$

then the plastic strain rate exceeds $\dot{\gamma}_t$ essentially everywhere in the active plastic zone.

The effect of increasing the material rate sensitivity at a fixed crack velocity can be seen in Fig. 10(b). The curve for $Q \to \infty$ is the perfectly plastic result (4.7) of Ref. [23]. The smaller Q is, the greater the rate effect. One way to think of this is that as G decreases with m fixed, the size of the active plastic zone decreases and the portion of the zone dominated by the high strain rate regime increases, as indicated by eqn (4.12). Alternatively, if G and m are regarded as fixed, then Q decreases with decreasing $\dot{\gamma}_0$, corresponding to increasing strain rate sensitivity. Then, ζ also increases but its effect on the solution in the range of small ζ is of secondary importance.

Curves of G_{tip}/G as a function of m are shown in Fig. 11(a) for several values of Q with $\zeta = 0.01$. The points are from the numerical calculations; the solid-line curves are the predictions from the asymptotic formula (3.17); and the dashed-line curves are obtained from a slight modification of the asymptotic formula. The modified formula reproduces the numerical results with high accuracy over the range of parameters in which calculations have been made. The motivation for the modification is now described. The asymptotic result [eqn (3.12)] for the

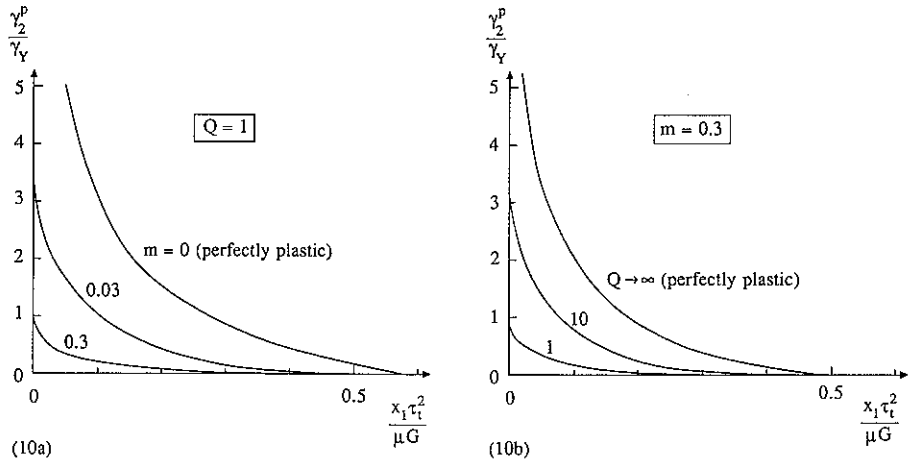

Fig. 10. Plastic strain distributions ahead of crack tip in mode III. (a) For fixed Q and various m; (b) for fixed m and various Q.

plastic dissipation and the ensuing asymptotic formulae [eqn (3.17)] for G_{tip}/G were derived using the near-tip stress field [eqn (3.8)] with amplitude K_{tip} to calculate the plastic strain rates. The modification is obtained if, instead, one uses the stress field (3.8) with the amplitude $(KK_{tip})^{1/2}$, which is the "harmonic mean" of K_{tip} and K. With this change, eqn (3.12) for the plastic dissipation still holds but with G_{tip}^2 replaced by GG_{tip}, and eqn (3.17) becomes

$$G_{tip} = G - H(m)\left(\frac{\dot{\gamma}\mu^2}{\tau_t^3 v}\right) GG_{tip}. \qquad (4.13)$$

This modified formula still retains its asymptotic validity in the limit of small plastic dissipation since $G_{tip} \to G$ in this limit. The significantly improved accuracy of eqn (4.13) reflects the fact that the singular stress field with amplitude K_{tip} underestimates the stresses while $(KK_{tip})^{1/2}$ represents a choice between K_{tip} and K. The modified formula is still restricted to the range in which most plastic dissipation occurs in the high strain rate regime. Although it correctly predicts that $G_{tip}/G \to 0$ as $v \to 0$, it does not provide an accurate transition to the rate-independent case since in this limit essentially all dissipation occurs with $\dot{\gamma}^p < \dot{\gamma}_t$.

With $\dot{\gamma}$ defined by eqn (3.14), G_{tip}/G from eqn (4.13) can be expressed in terms of the parameters in

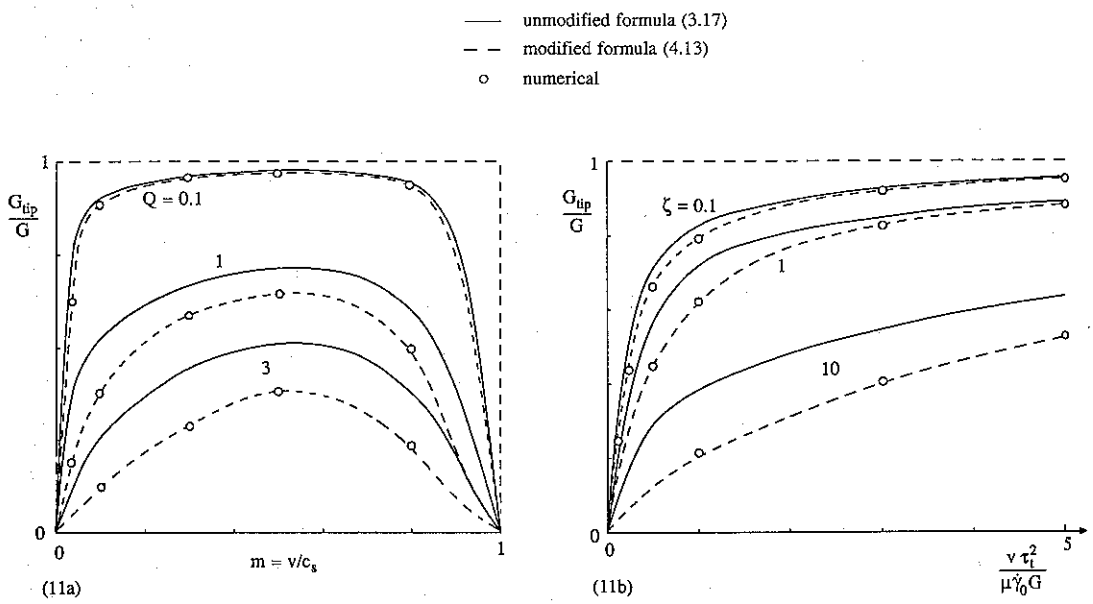

Fig. 11. Comparison of mode III numerical results to asymptotic formulae for G_{tip}/G as a function of m. (a) Dynamic results for $\zeta = 0.01$ and various Q; (b) inertia-free results for various ζ.

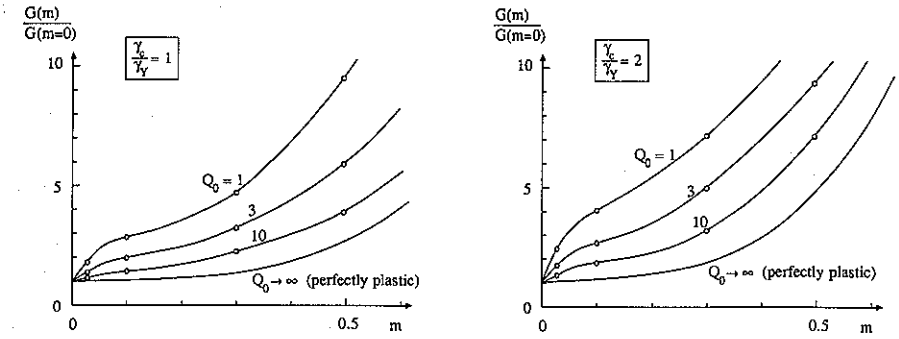

Fig. 12. Value of G needed to drive crack at normalized crack speed m in rate-sensitive material compared to quasistatic value $G(m=0)$. (a) For $\zeta=0.01$, $\gamma_c/\gamma_Y=1$ and various Q_0; (b) for $\zeta=0.01$, $\gamma_c/\gamma_Y=2$ and various Q_0.

eqn (4.11) as

$$\frac{G_{tip}}{G}=\left[1+\frac{1}{6}\frac{H(m)}{m}(1+2\zeta)Q\right]^{-1}. \quad (4.14)$$

For $m<0.3$ inertia is relatively unimportant in this relation. Using $H(m)\cong H(0)=4/\pi$ from eqn (3.20), one finds from eqn (4.13) that in the inertia-free limit

$$\frac{G_{tip}}{G}=\left[1+\frac{4}{\pi}\frac{\dot{\gamma}\mu^2 G}{\tau_t^3 v}\right]^{-1}=\left[1+\frac{2}{3\pi}(1+2\zeta)\frac{\mu\dot{\gamma}_0 G}{\tau_t^2 v}\right]^{-1}, \quad (4.15)$$

where the latter expression holds for the case of linear high strain rate behavior. Figure 11(b) shows the comparison between eqn (4.15) and numerical calculations carried out with inertia neglected in the formulation.

We end this section by showing results for the effect of strain rate sensitivity on the propagation of a crack in mode III when the *strain-based* propagation criterion (4.3) is imposed on the solution to model crack advance by the *micro-void mechanism*. We defer discussion of application to cleavage cracking until the next section when mode I is considered. Curves giving the value of G needed to drive the crack in steady-state with the criterion (4.3) met are plotted in Fig. 12, with $\gamma_c/\gamma_Y=1$ in Fig. 12(a) and $\gamma_c/\gamma_Y=2$ in Fig. 12(b). The curves are derived from the plastic strain distributions such as those in Fig. 10. The G-value in Fig. 12 is normalized by the quasi-static, steady-state G-value for driving the crack [i.e. $G(m=0)$ from eqn (4.10) with $\tau_Y\equiv\tau_t$]. Each curve in Fig. 12 corresponds to a prescribed value of the parameter

$$Q_0\equiv\frac{\mu\dot{\gamma}_0 G(m=0)}{c_s\tau_t^2}=1.69\frac{x_c\dot{\gamma}_0}{c_s}\exp\{(1+2\gamma_c/\gamma_Y)^{1/2}-1\}, \quad (4.16)$$

together with $\zeta=0.01$. The curves in Fig. 12 are otherwise independent of x_c.

The lowest curve, corresponding to $Q_0\to\infty$, is the rate-independent result which was also shown in Fig. 8. The material rate-sensitivity has its greatest effect at relatively low values of m; at values of m above about 0.3 inertial effects become important. Analogous behavior is reported in Ref. [26] for a mode III study which used a visco-plastic formulation of rate-sensitivity based on an over-stress model.

The mode III model implies that material rate-sensitivity significantly increases the resistance to high speed crack growth when crack advance occurs by a mechanism such as micro-void coalescence which requires a critical level of strain in the fracture process zone.† The effect is easy to understand. The faster the crack runs, the higher must be the general stress level in the active plastic zone to achieve the critical strain level. This, in turn, requires a higher crack driving force. It will be seen that the effect of rate-sensitivity on crack advance by cleavage is quite different.

The values of γ_c/γ_Y used to generate the curves in Fig. 12 are unrealistically small; these choices were dictated by the range of accurate results available from our numerical calculation. Nevertheless, the trends of the model for larger γ_c/γ_Y are clear. An experimental study of dynamic crack propagation in a high strength aluminum alloy [28] reveals the strong dependence of K on crack velocity in the range of relatively low velocities for which inertial effects are not very important (i.e. $m<0.3$). The strain rate sensitivity of aluminum is very weak in the low to moderate strain-rate region for $\dot{\gamma}^p<10^3\,s^{-1}$, and the elastic-perfectly plastic representation used here for

† For the purpose of discussion it is assumed that this strain level is not a strong function of crack velocity. Some ideas on the role of strain rate on the micro-void fracture process itself have been advanced in Ref. [27].

that regime is appropriate. Moreover, there is ample evidence [12] that aluminum has strong rate-sensitivity above about $10^3\,s^{-1}$.

5. STEADY-STATE CRACK GROWTH IN PLANE STRAIN, MODE I WITH APPLICATION TO CLEAVAGE

5.1. *Numerical results*

Numerical calculations for the plane strain, mode I problem have been made [6] for the material characterized by the linear high-strain rate relation (2.2). With $\dot{\gamma}$ defined by eqn (3.14), the modified formula (4.13) can be rewritten as

$$\frac{G_{tip}}{G}=\left[1+\tfrac{1}{6}H(m)(1+2\zeta)\frac{\mu\dot{\gamma}_0 G}{v\tau_i^2}\right]^{-1}, \quad (5.1)$$

and this formula applies to both mode III and mode I with the appropriate choice for $H(m)$. A comparison of the numerical results with predictions from the two analytical formulae (3.17) and (5.1) is given in Fig. 13, and this figure may be contrasted with the corresponding comparison for mode III in Fig. 11(a). The numerical results are in close agreement with the modified formula (5.1) at high velocities but fall roughly halfway between the predictions of the two formulae in the range of low m. A more extensive comparison involving all the numerical results obtained in mode III and mode I is given in Fig. 14. To reveal in the most convincing way the predictive capability of the modified result [eqn (5.1)], we have plotted the numerical results, as well as the unmodified prediction from eqn (3.17), as G_{tip}/G against

$$\left[1+\tfrac{1}{6}H(m)(1+2\zeta)\frac{\mu\dot{\gamma}_0 G}{v\tau_i^2}\right]^{-1}. \quad (5.2)$$

In the case of mode III the agreement with eqn (5.1) is excellent for all m-values for G_{tip}/G as small as 0.1. For mode I the agreement with eqn (5.1) is not quite as good when G_{tip}/G is below 0.5 and when $m \leq 0.3$. Clearly the unmodified formula (3.17) consistently underestimates the plastic dissipation (i.e. overestimates G_{tip}/G) while the modified formula (5.1) or (4.13) tends to overestimate the dissipation, although not by much except at low values of G_{tip}/G and at low m.

5.2. *Application to a running cleavage crack*

For a crack running fast enough such that most of the plastic strain accumulates in the high strain rate regime, the relation between G_{tip} and G is given approximately by the asymptotic formula (3.17) or its modification (4.13) with $H(m)$ plotted in Fig. 5. For the purposes of discussion, it will be assumed that the material is characterized by the linear representation (2.2) in the high strain rate regime, but the discussion could equally be based on the more elaborate representation (2.3). The discussion which follows will be based on the modified formula (5.1), together with the numerical results themselves.

Under the assumption that the energy consumed by the cleavage fracture process is separable from the plastic dissipation occurring outside the fracture

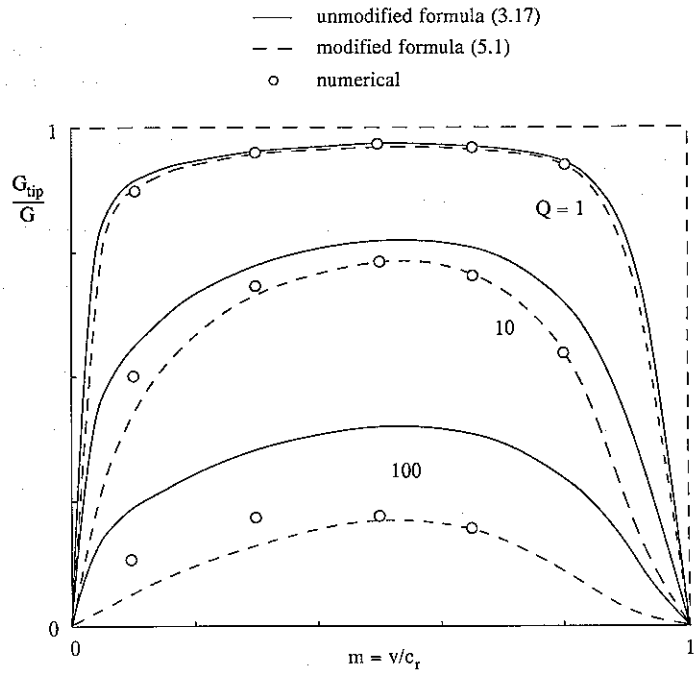

Fig. 13. Comparison of mode I plane strain dynamic numerical results to asymptotic formulae for G_{tip}/G as a function of m ($\zeta = 0.01$, $\nu = 0.29$).

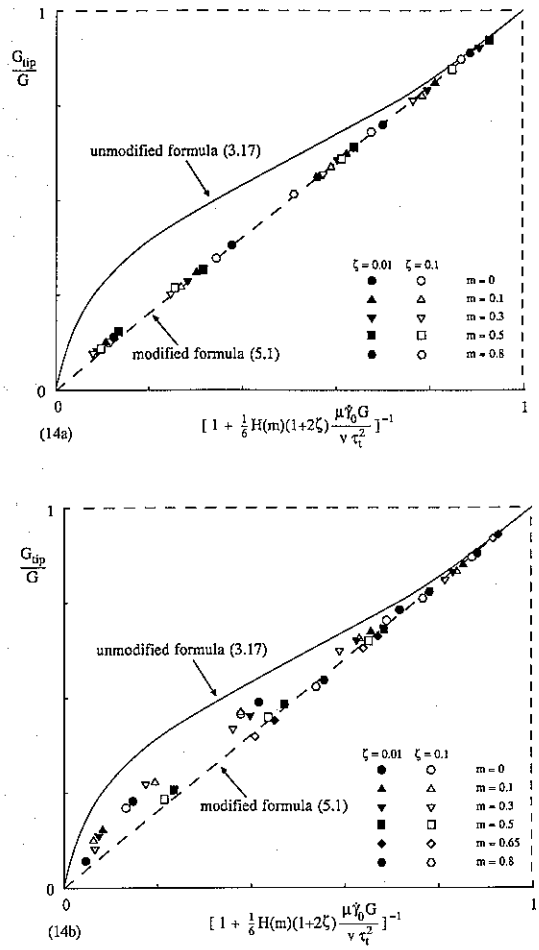

Fig. 14. Comparison of numerical results to asymptotic formulae for G_{tip}/G as a function of the quantity $[1+\frac{1}{6}H(m)(1+2\zeta)\mu\dot{\gamma}_0 G/v\tau_t^2]^{-1}$ for all values of m, Q and ζ. (a) mode III; (b) mode I plane strain ($\nu = 0.29$).

process zone, the condition for continuing propagation of a running cleavage crack is

$$G_{tip} = G^c_{tip}(T, v), \tag{5.3}$$

where G^c_{tip} is the energy per unit area of crack advance associated with the fracture process. Under idealized "lattice cleavage" one might assume that G^c_{tip} is not strongly dependent on either temperature T or crack velocity. But for cleavage cracking of polycrystalline metals, and even for cleavage of single crystals, the fracture process is rarely a simple cleaving of the atomic lattice. For example, the cleaved surfaces of single crystals of iron [29] and tungsten [30] are covered with river patterns which clearly indicate that G^c_{tip} cannot be taken as simply twice the surface energy of the crystal. Estimates of G^c_{tip} for single crystals of iron are usually 10 to 20 times the surface energy. Moreover, the surface features tend to become more prominent, and evidently more dissipative, the higher the temperature. This trend is even more apparent in polycrystalline metals which cleave, such as silicon iron [31] and carbon steels [32, 33] below the ductile–brittle transition. The advance of the macro-crack involves the nucleation of a multitude of grain-sized micro-cleavage cracks in a fracture process zone which is many grain diameters in extent. The final separation of the crack flanks requires a fracturing of the remaining ligaments bridging the micro-cracks. At low temperatures the ligament fracture is observed to occur by cleavage on less favorably orientated cleavage planes accompanied by some plastic deformation of the ligaments [32]. At higher temperatures approaching the ductile–brittle transition, the ligaments often fail by micro-void nucleation and coalescence with extensive plastic straining. This combination of cleavage and the micro-void mechanism is sometimes referred to as quasi-cleavage. Even though a high fraction of the fracture surface has been cleaved, most of the energy consumed by the fracture process goes into deforming and rupturing the ligaments. Estimates of G^c_{tip} for cleavage of typical structural steels, such as that discussed below, are of the order of a thousand times the surface energy of iron. To date there has been little effort to develop micro-mechanical models for $G^c_{tip}(T, v)$ for either single crystal or polycrystalline materials. One exception is a study on steel [33].

To illustrate application of the energy balance equation (5.1) to cleavage crack propagation, it will be assumed that G^c_{tip} is a function of temperature but not of crack velocity. The actual velocity dependence of G^c_{tip} is likely to be significant, especially in polycrystalline materials where the ligament breaking should be strongly velocity dependent as discussed further below. However, there is little information available at the present time to estimate this dependence.

By imposing the propagation criterion (5.3) on (5.1), one finds

$$\frac{G}{G^c_{tip}} = [1 - D(m)P_c]^{-1}, \tag{5.4}$$

where P_c is a temperature dependent, non-dimensional *material parameter* given by

$$P_c = \tfrac{1}{3}(1+2\zeta)\frac{\mu\dot{\gamma}_o G^c_{tip}}{c_s\tau_t^2} = \frac{1}{3}\left(1 + \frac{2\dot{\gamma}_t\mu}{\dot{\gamma}_0\tau_t}\right)\frac{\mu\dot{\gamma}_0 G^c_{tip}}{c_s\tau_t^2} \tag{5.5}$$

and

$$D(m) = \frac{1}{2}\frac{H(m)}{m}\frac{c_s}{c_r}. \tag{5.6}$$

The function $D(m)$, which was given in Ref. [7], is included here in Fig. 5 and in Table 2.

Inspection of eqn (5.4) reveals that the propagation criterion cannot be met if P_c is larger than a critical value. For $\nu = 0.29$ the minimum value of

$D(m)$ is 0.109, and thus P_c cannot exceed 9.17. Moreover, when P_c is large, but below 9.17, the range of crack velocities for which propagation is possible is restricted to m-values satisfying $D(m)P_c < 1$. The prediction of a *critical value* of the material parameter P_c above which cleavage is not possible is a consequence of the modified energy balance formula. This is evident in Fig. 15 where the numerical results from Fig. 14 have been used to plot values of G^c_{tip}/G as a function of $D(m)P_c$. It is seen that the cut-off at $D(m)P_c = 1$ predicted by eqn (5.4) is not a feature of the numerical results. In other words, the numerical results do not indicate that cleavage will necessarily be excluded for values of P_c greater than some critical value. On the other hand, using the empirical upper envelope of all the numerical results which is shown in Fig. 15, we will show later that cleavage is effectively excluded at sufficiently large P_c.

To illustrate the prediction of crack arrest for a crack propagating according to the criterion (5.3), imagine the crack is running into a pre-stressed block and assume that reflected waves have not yet reached the crack tip. Let G_S be the quasi-static energy release rate of a crack whose length coincides with that of the running crack. The approximate relation between G and G_S is given by eqn (3.6). The equation for the propagation velocity of the crack ($m = v/c_r$) follows from eqn (5.4) as

$$\frac{G_S}{G^c_{tip}} = \frac{1}{1-m}[1 - D(m)P_c]^{-1}. \tag{5.7}$$

The prescribed loads and current crack length enter this equation through G_S, and it is in this manner that the small scale yielding energy balance at the crack tip is coupled to the applied loads and overall geometry. More complicated problems, including the arrival of reflected waves at the tip, will generally require a numerical solution for the history of G.

Curves of G_S/G^c_{tip} vs m for various values of P_c are plotted in Fig. 16. The curve for $P_c = 0$ corresponds to the propagation of a perfectly brittle crack involving no plastic dissipation. As long as $G_S > G^c_{tip}$ the crack will propagate, and crack velocity increases monotonically with G_S. When plastic dissipation occurs (i.e. $P_c > 0$) the crack cannot propagate if G_S/G^c_{tip} does not exceed the minimum shown in Fig. 16. Furthermore, the slowest velocity for which propagation can be sustained is the value m^* associated with $(G_S/G^c_{tip})_{min}$. The left-hand branch of the curve of G_S vs m corresponds to unsustainable (or unstable) propagation in the sense that any perturbation which slows the crack can readily be shown to cause G to drop below G^c_{tip} and thus arrest the crack. Similar considerations have been discussed in Ref. [27]. The minimum of G_S/G^c_{tip} and the minimum of sustainable propagation velocity m^* is plotted against P_c in Fig. 17. Also shown in Fig. 17 are the corresponding curves derived from the empirical upper envelope to the numerical results in Fig. 15.

For a crack propagating into a prestressed body such that G_S/G^c_{tip} decreases with increasing crack length, propagation cannot be sustained when G_S/G^c_{tip} falls below $(G_S/G^c_{tip})_{min}$. Moreover, arrest is expected to occur abruptly, essentially from m^* to zero velocity and not by a gradual slowing of the crack to zero velocity as was seen to be possible for crack advance by the micro-void mechanism. Of course, the arrest process is transient, and not steady-state. But the fact that steady-state propagation is not possible in the range $0 \le m < m^*$ strongly suggests that the transient arrest process is associated with a very small amount of crack advance, probably much less than the extent of the active plastic zone. Experimental evidence for abrupt arrest of cleavage cracks is not extensive. Recent data [34] on cleavage cracking of wide plates, with the crack running against a temperature gradient, suggests that abrupt arrest may occur. Early

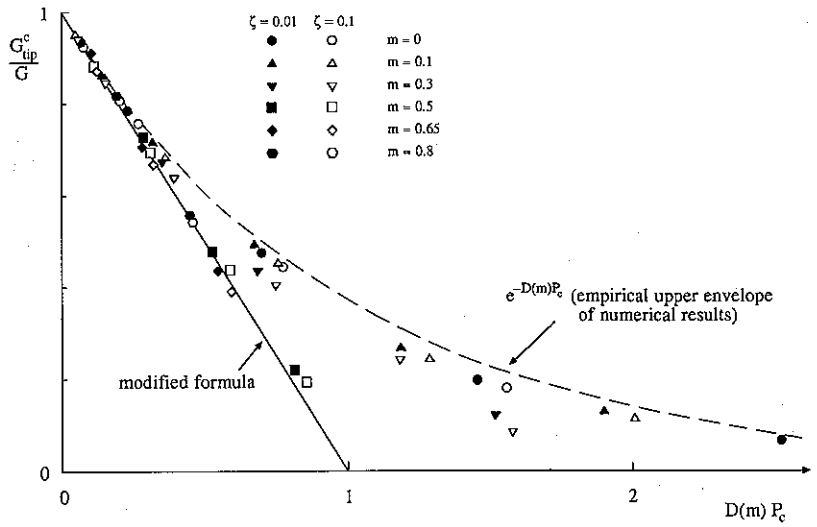

Fig. 15. Comparison of numerical results and modified asymptotic formula (5.1) for G^c_{tip}/G as a function of $D(m)P_c$. Also shown is an empirical upper envelope to the numerical results.

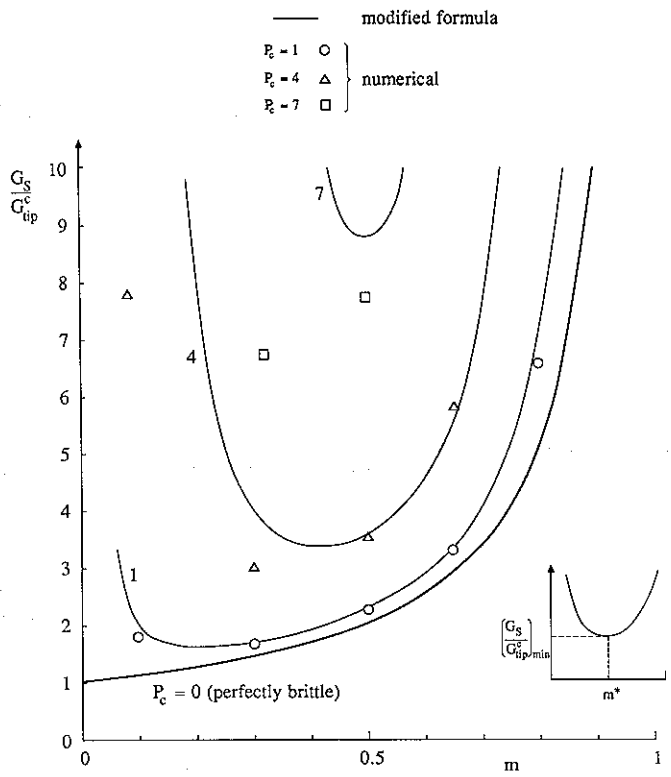

Fig. 16. G_S/G^c_{tip} as a function of m for various P_c ($\zeta = 0.01$, $\nu = 0.29$), as predicted by the modified formula (5.1).

crack arrest tests [35] in rate-sensitive brittle plastic materials do strongly suggest abrupt arrest with the minimum propagation velocity increasing with increased rate-sensitivity, in accord with the present predictions.

Another basic point about cleavage crack propagation which can be inferred from the above example is that, while the relation between G and v is material specific, it is not strictly correct to speak of the crack arrest toughness K_{Ia} or, equivalently, G_{Ia} as a *material property*. Given a propagation relation of the form G vs m such as eqn (5.4), the value of G at arrest is not independent of the prescribed loading history. The arrest value of G in the example above was associated with the minimum value of G_S since G_S was prescribed and *not* G. Other loading histories or configurations will generally lead to other relations between G and the prescribed quantities, and thus G at arrest may differ somewhat from the example above. If arrest occurs at relatively low values of m, these differences will be small and possibly unimportant.

5.3. *An illustrative example*

An illustration which brings out the influence of temperature on the material parameter P_c and its effect on the arrest level of G is presented in Fig. 18 for cleavage of mild steel. The temperature dependence of the transition stress τ_t of a fine grained mild steel shown in Fig. 18(a) was developed from Refs [9] and [13] as discussed in more detail in Ref. [7]. From the data of Ref. [9] we also chose

$$\dot{\gamma}_t = 5 \times 10^3 \mathrm{s}^{-1} \quad \text{and} \quad \dot{\gamma}_0 = 3 \times 10^7 \mathrm{s}^{-1} \tag{5.8}$$

and these were taken to be independent of T as suggested by the data. The value of G^c_{tip} at absolute zero was taken as

$$G^c_{tip}(0\,\mathrm{K}) = 1.73 \times 10^3\,\mathrm{Jm}^{-2} \tag{5.9}$$

giving, from eqns (5.7) and (3.6),

$$G_{Ia}(0\,\mathrm{K}) = (1 - m^*)(G_S)_{min} = 2.0 \times 10^3\,\mathrm{Jm}^{-2}, \tag{5.10}$$

which is representative of the arrest value of mild steel at very low temperatures. The temperature dependence of μ was taken from Ref. [13]. The parameter ζ was less than 0.1 and was neglected. To illustrate the temperature dependence of $G^c_{tip}(T)$ we have considered (arbitrarily, since actual data or estimates are not available) the three dependences labeled (A), (B) and (C) in Fig. 18(b). Case (A) assumes G^c_{tip} is independent of T, while the other two assume the fracture process consumes more energy as T increases. The corresponding temperature variations of P_c computed from the temperature variations of τ_t, μ and G^c_{tip} are shown in Fig. 18(c).

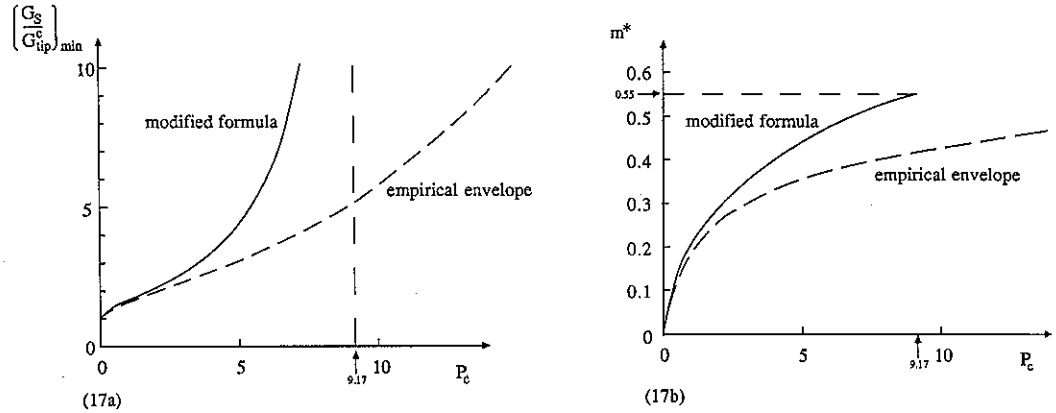

Fig. 17. Minimum value of G_S needed to drive the crack dynamically and associated value of m as functions of P_c ($\zeta = 0.01$, $\nu = 0.29$) as predicted by the modified formula (5.1) and by the empirical envelope of Fig. 15.

Finally, in Fig. 19, the temperature dependence of the arrest value,

$$G_{Ia} = (1 - m^*)(G_S)_{min},$$

is plotted as a solid-line curve for the three cases, where $(G_S)_{min}$ and m^* are obtained from P_c using Fig. 17. In each case, the temperature above which cleavage cannot occur corresponds to the temperature at which $P_c = 9.17$. The relatively minor differences in the temperature variations of G^c_{tip} over the three cases give rise to fairly significant shifts in the temperature above which cleavage is excluded. As already emphasized, we expect these predictions to overestimate the G_{Ia} at a given temperature since the modified formula tends to overestimate the plastic dissipation. The second set of curves in Fig. 19 (the dashed-line curves) were generated using the empirical upper envelope to the numerical results shown in Fig. 15. These curves are expected to underestimate G_{Ia}, and thus the two sets of predictions should serve to bracket results from a full calculation. If there is some modest temperature variation of G^c_{tip}, as in cases (B) or (C), then G_{Ia} is predicted to rise dramatically within a fairly narrow range of temperature corresponding to P_c attaining values of about 10. While cleavage may not be strictly excluded above some critical temperature (as the modified formula predicts), there is nevertheless a fairly abrupt upturn in the crack arrest toughness which is due to the increased plastic dissipation associated with increasing temperature.

5.4. *Extensions and alternatives*

The above discussion was based on the linear representation in the high strain rate regime, but other representations can be accommodated and will lead to qualitatively similar predictions. For example, the derivations go through in precisely the same way for the more elaborate power law representation (2.3) where $\dot{\bar{\gamma}}$ is given by eqn (3.15). Formulae (5.4) and (5.7) continue to hold if P_c is defined as

$$P_c = 2\dot{\bar{\gamma}}\mu^2 G^c_{tip}/(c_s\tau_i^3). \tag{5.11}$$

The Bodner-Partom visco-plastic model (see Ref. [15], p. 228) has been used in an analysis of cleavage crack propagation in a pressure vessel steel [36]. That analysis is similar in most respects to the present one with qualitatively similar results.

In the illustrative examples discussed above the velocity dependence of G^c_{tip} has been ignored. It seems likely that there is a strong velocity dependence associated with the cleavage fracture process, particularly in polycrystalline materials. Indirect evidence for this dependence can be inferred from the fact that the visco-plastic theory presented here predicts higher crack velocities than are usually observed. For example, it is seen in Fig. 16 that crack velocities of approximately one half the Rayleigh wave speed (i.e. $m \cong 1/2$) are implied when visco-plasticity is substantial. Crack velocities in steels undergoing cleavage cracking are seldom reported to be this high, and velocities as low as one tenth the Rayleigh speed are frequently observed. The micro-mechanics of the temperature and velocity dependence of G^c_{tip} remain to be explored. We speculate that the velocity dependence of G^c_{tip} at a fixed temperature may have the form shown in Fig. 20. As the crack velocity increases there is some evidence that an increasing profusion of micro-cracking occurs accompanied by increasing roughness of the fracture surface of the macro-crack. Moreover, at temperatures in the quasi-cleavage range the energy absorbed by the remaining ligaments may increase with strain rate (and thus velocity) because of the tendency for flow localization to be retarded at a very high strain rates. Thus, G^c_{tip} may be an increasing function of velocity for velocities which are not too small. If so, this would help to reconcile experi-

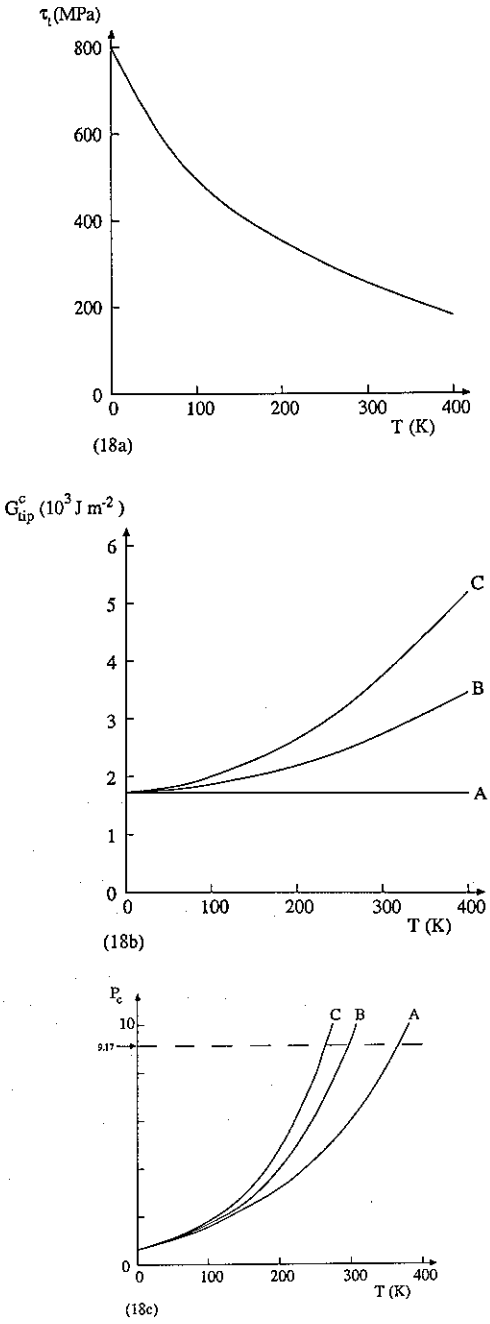

Fig. 18. Representative temperature dependence of material properties for mild steel. (a) τ_i; (b) three postulated temperature variations of G^c_{tip}; (c) consequent variations of P_c.

mentally observed crack velocities with predictions of the theory.

6. A DISLOCATION DYNAMICS MODEL OF HIGH STRAIN RATE CRACK GROWTH IN PLANE STRAIN, MODE I

In this section we re-examine the same problem addressed in the previous section using dislocation modeling. We consider the interaction of a rapidly propagating crack with pre-existing dislocations in an otherwise elastic material. First, the interaction of the crack with a single dislocation will be considered with the geometry indicated in Fig. 21. The crack is assumed to propagate with velocity v through the material and to pass within the vicinity of an edge dislocation that is restricted to a specific glide plane. The stress field associated with the dynamic stress intensity factor induces a shear stress on the glide plane which is taken as the driving force for the dislocation motion. An equation of motion for the dislocation is adopted, and the energy dissipated through the dislocation glide is computed. Finally, it is assumed that the moving crack encounters a distribution of like dislocations spread over the plane, and the total energy dissipation per unit crack advance is estimated. The analysis is not exact; approximations or assumptions are introduced at various stages. Nevertheless, the end result is an energy balance which has a similar form to that discussed above and which permits the continuum formulae to be reinterpreted in dislocation theory terms.

6.1. *The crack–dislocation model*

Consider a mode I crack growing steadily at speed v in the x_1-direction under plane strain conditions in a linear isotropic elastic solid. The stress field near the tip of the crack is given by eqn (3.1) where K is the dynamic stress intensity factor. The position and orientation of the dislocation relative to the crack are shown in Fig. 21. The glide plane of the dislocation is inclined to the plane of the crack at an angle ω, and the unit normal to the glide plane is $n_i = (-\sin\omega, \cos\omega)$. The crack tip crosses the glide plane at time $t = 0$, and the position of the dislocation core is specified by its distance $u(t)$ from the crack plane. The polar coordinates r, θ are now used to specify the position of the dislocation with respect to the crack tip. These equivalent but alternate descriptions of the position of the dislocation are related by

$$u(t)\sin\omega = r\sin\theta,$$
$$u(t)\cos\omega = r\cos\theta + vt. \tag{6.1}$$

Of fundamental importance in analyzing the motion of the dislocation is the shear traction on the glide plane

$$S_i = \sigma_{ij}n_j - \sigma_{jk}n_k n_j n_i. \tag{6.2}$$

The magnitude of S_i (with due regard to sense), say $\tau(r,\theta) = \pm\sqrt{(S_x^2 + S_y^2)}$, is the resolved shear stress on the glide plane. The resolved shear stress may alternatively be expressed as a function of u and t by means of

$$r = \sqrt{u^2 - 2uvt\cos\omega + v^2t^2},$$
$$\theta = \tan^{-1}\left(\frac{u\sin\omega}{u\cos\omega - vt}\right), \tag{6.3}$$

which follows directly from eqn (6.1).

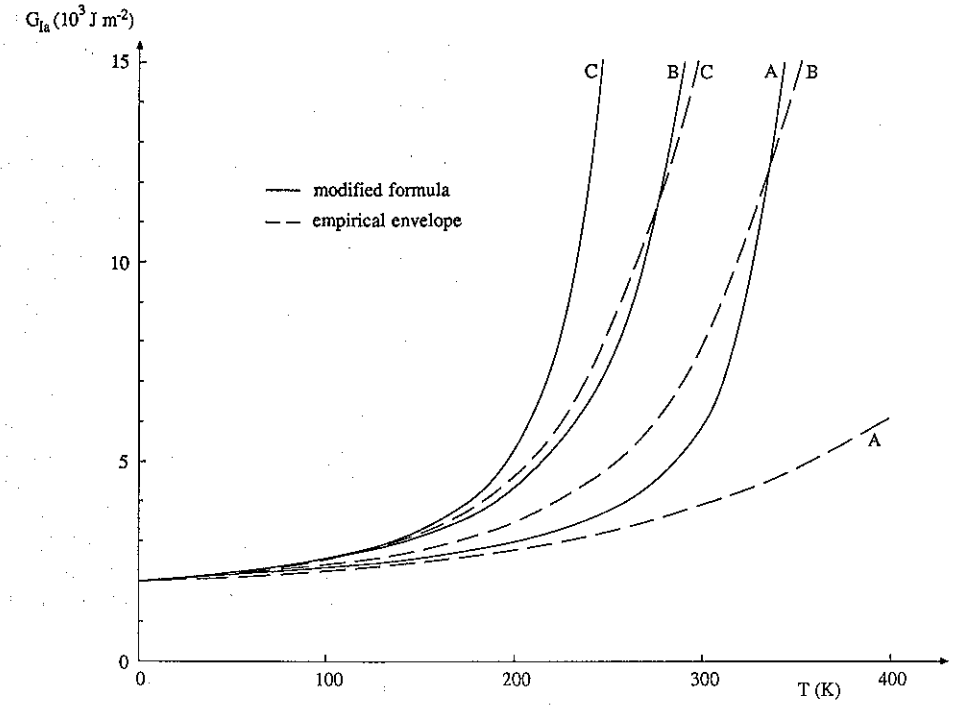

Fig 19. Value of G immediately prior to arrest as function of temperature, as predicted by modified result (5.1) and by empirical envelope of Fig. 15.

An equation of motion for the dislocation is next developed. The idea that the resolved shear stress on the glide plane at the dislocation core provides the driving force, a common viewpoint in the area of dislocation dynamics, is adopted. First, it is assumed that the magnitude of the resolved shear stress must exceed a certain value, say τ_i, in order to produce any high velocity dislocation motion. In addition, it is assumed that the velocity $\dot{u}$ is proportional to the resolved shear stress. An equation of motion having these properties is

$$B\dot{u} = \begin{cases} b\tau & \text{if } |\tau| \geq \tau_i \\ 0 & \text{if } |\tau| < \tau_i \end{cases}, \tag{6.4}$$

where b is the magnitude of the Burgers vector of the dislocation, and B is a drag coefficient reflecting viscous resistance of the lattice to dislocation motion at low and moderate dislocation speeds. The right side of eqn (6.4) is the familiar Peach–Koehler force of dislocation mechanics.

The equation of motion suggested in eqn (6.4) implies no restriction on the maximum attainable dislocation velocity as the applied resolved shear stress is increased. The equation of motion may be modified to incorporate the condition that as the shear stress becomes indefinitely large, then the dislocation speed approaches the Rayleigh wave speed of the material. An equation of motion having this additional property is:

$$B\dot{u} = \frac{b\tau}{(1+\tau^2/\tau_r^2)^{1/2}} \quad \text{if} \quad |\tau| \geq \tau_i, \tag{6.5}$$

and $\dot{u} = 0$ otherwise, where $\tau_r = c_r B/b$. The equation of motion could be modified further to incorporate the idea that it is only the *excess* of the resolved shear

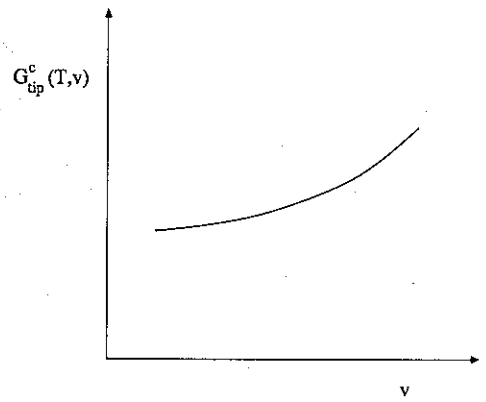

Fig. 20. Speculative form of velocity dependence of G^c_{tip}.

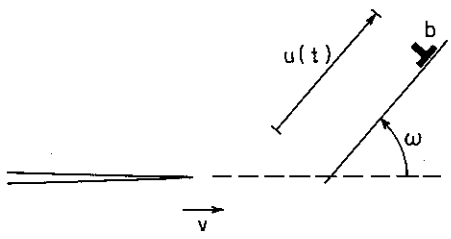

Fig. 21. Geometry for analysis of dislocation interaction with propagating crack.

stress *above* the critical stress τ_i that drives the dislocation. The results of the calculations described here were obtained on the basis of the form in eqn (6.4).

An equation of motion of the form (6.4) or (6.5) presumes that the primary resistance to dislocation motion is a drag which may be described phenomenologically as a viscous drag. It has been shown in Ref. [37] and elsewhere that, for transient motion of a dislocation in an elastic medium, the motion of the dislocation through its own radiated stress field results in a resistance which depends on the history of the motion. If the kinematic variable used to describe the motion is an analytic function of time, then the history is included in a Taylor expansion about the current instant. Further, if the expansion is truncated after the second derivative term for one reason or another (e.g. uniformly accelerated motion), then the resistance includes a contribution that is proportional to the acceleration of the dislocation. In analogy with Newton's Second Law of Particle Mechanics the coefficient of the acceleration term is identified as an effective mass of the dislocation. This point of view is not pursued further here because dislocation motion under the conditions imagined is not expected to include rapid changes in speed or high accelerations and it is expected to be adequately described by the viscous drag mechanism.

6.2. *Energy dissipated in interaction*

For a given level of crack tip stress intensity K and crack speed v, the following nondimensional physical parameters are introduced:

$$\bar{\tau} = \tau/\tau_i, \quad \bar{\tau}_r = \tau_r/\tau_i, \quad \bar{u} = u/(K/\tau_i)^2,$$

$$\bar{t} = vt/(K/\tau_i)^2, \quad \bar{B} = Bv/\tau_i b, \quad \bar{r} = r/(K/\tau_i)^2. \quad (6.6)$$

The dislocation equation of motion takes the form

$$\bar{B}\frac{\mathrm{d}\bar{u}}{\mathrm{d}\bar{t}} = \begin{cases} \bar{\tau} & \text{if } |\bar{\tau}| \geq 1 \\ 0 & \text{otherwise} \end{cases}, \quad (6.7)$$

where $\bar{\tau}$ is understood to be a function of $\bar{r}, \theta$. These quantities, in turn, may be expressed in terms of $\bar{u}, \bar{t}$ through nondimensionalized forms of eqn (6.3) as

$$\bar{r} = \sqrt{\bar{u}^2 - 2\bar{u}\bar{t}\cos\omega + \bar{t}^2}$$

$$\theta = \tan^{-1}\left(\frac{\bar{u}\sin\omega}{\bar{u}\cos\omega - \bar{t}^2}\right). \quad (6.8)$$

Consequently, eqn (6.7) is an ordinary differential equation of the form

$$\frac{\mathrm{d}\bar{u}}{\mathrm{d}\bar{t}} = F(\bar{u}, \bar{t}), \quad (6.9)$$

where the right hand side is given implicitly through eqn (6.8). The differential equation is subject to the initial condition that $u(t_0) = u_0 = y_0/\sin\omega$ where it is assumed that $\omega \neq 0$ and t_0 is the time at which the resolved shear stress magnitude at the initial position of the dislocation is first elevated to τ_i by the approaching crack edge. The differential equation has been integrated numerically by a standard fourth order Runge–Kutta procedure.

In order to carry out a calculation, values of system parameters must be selected. The following values are selected as being representative:

$$B = 10^{-5}\,\mathrm{Pa\cdot s}, \qquad \tau_i = 10^2\,\mathrm{MPa},$$

$$b = 3\times10^{-10}\,\mathrm{m}, \quad c_r = 3\times10^3\,\mathrm{ms}^{-1}. \quad (6.10)$$

For these values, $\bar{\tau}_r \approx 1$, which implies that the dislocation equation of motion (6.5) deviates from a linear relationship between resolved shear stress and dislocation speed at moderate dislocation speeds.

With values of the parameters and initial data specified, the differential equation (6.7) can be solved. The detailed features of the solution are not of particular interest, except to note that the dislocation speed was found to be a small fraction of c_r unless the crack speed approached this wave speed. Typically, the maximum dislocation speed was about equal to the crack tip speed. Of primary interest is the energy dissipated through dislocation motion during the interaction. The rate of energy dissipation on the glide plane (per unit thickness in the direction normal to the xy-plane) is defined as the rate of work of the driving force on the dislocation τb acting through the dislocation speed $\dot{u}$. If the total energy dissipated in the interaction is denoted by $w(y_0, \omega)$ for a particular glide plane and particular initial position y_0 then

$$w(y_0,\omega) = \int_{-\infty}^{+\infty} \tau b\dot{u}\,\mathrm{d}t = \frac{K^2 b}{\tau_i}\int_{-\infty}^{+\infty}\bar{\tau}\frac{\mathrm{d}\bar{u}}{\mathrm{d}\bar{t}}\,\mathrm{d}\bar{t}$$

$$= \frac{K^2b^2}{vB}\int_T \bar{\tau}^2\,\mathrm{d}\bar{t} = \frac{K^2b^2}{vB}\bar{w}(\bar{y}_0,\omega), \quad (6.11)$$

where T is the union of time intervals over which $|\bar{\tau}| \geq 1$. The coefficient of the dimensionless quantity $\bar{w}$ has a simple interpretation. It is the work done as a dislocation with Burgers vector b moves steadily under the action of a driving force $\tau_i b$ at speed $\dot{u} = \tau_i b/B$ during the time that the crack advances a distance $(K/\tau_i)^2$ at speed v.

6.3. *A distribution of dislocations*

Suppose now that the growing crack encounters a uniform distribution of dislocations. The dislocation lines are all parallel to each other and normal to the xy-plane so that the model is still within the framework of plane strain deformation. The number of dislocations piercing the xy-plane per unit area is N. If it is assumed that the dislocations do not interact then the energy dissipated as the crack grows through the distribution is determined by summation

(in the form of integration in the present circumstances) over the distribution. Furthermore, with a view toward considering the result in terms of the fracture mechanics concept of energy release rate, the energy dissipated per unit crack advance is determined by integration only over the coordinate y_0 of the pre-existing distribution. Thus, the total mechanical energy dissipated per unit crack advance is:

$$W(N,\omega)=\frac{2NK^4b^2}{B v\tau_i^2}\int_0^\infty \bar{w}(\bar{y}_0,\omega)\,\mathrm{d}\bar{y}_0$$

$$=\frac{2NK^4b^2}{B v\tau_i^2}\,\bar{W}(\omega). \qquad (6.12)$$

The integral in eqn (6.12) has been evaluated numerically, using the result of the previous calculation on energy dissipated through motion of a single dislocation.

The result is now cast in terms of an overall energy balance as was done for the continuum model. The rate of energy flow per unit crack advance into the crack tip region is still denoted by G and is related to K by eqn (3.4). The rate of energy loss through the tip is denoted by G_{tip}, as before. In steady-state the energy balance is:

$$G_{tip}=G-W(N,\omega). \qquad (6.13)$$

Using eqns (6.12) and (3.4), we now rewrite this relation in a form which will permit immediate comparison with the corresponding continuum formula. Equation (6.13) becomes

$$G_{tip}=G-\tfrac{1}{6}\hat{H}(m)\left[\left(\frac{Nb^2\mu}{B}\right)\frac{\mu}{\tau_i^2 v}\right]G^2, \qquad (6.14)$$

where

$$\hat{H}(m)=48\,\bar{W}(\omega)/[(1-\nu)f(m)]^2. \qquad (6.15)$$

The continuum result [eqn (3.17)] for the linear high strain rate representation (2.2) is

$$G_{tip}=G-\tfrac{1}{6}H(m)\left[\frac{\dot{\gamma}_0\mu}{\tau_i^2 v}\right]G_{tip}^2, \qquad (6.16)$$

where $\zeta=\dot{\gamma}_i\mu/(\tau_i\dot{\gamma}_0)$ has been assumed negligible compared to unity.

To compare the two formulae note that for the linear continuum representation (2.2), $\mathrm{d}\dot{\gamma}^p/\mathrm{d}\tau=\dot{\gamma}_0/\mu$. Now consider for a moment the collection of terms Nb^2/B in eqn (6.14). According to Orowan's relation, the plastic shear strain rate due to N mobile dislocations per unit area, each with Burgers displacement b, moving at speed $\dot{u}$ is $Nb\dot{u}$. If the dislocation velocity is taken to depend linearly on applied shear stress with drag coefficient B as in eqn (6.4), then $\mathrm{d}\dot{\gamma}^p/\mathrm{d}\tau=Nb^2/B$. Thus, the factor $(Nb^2\mu/B)$ in eqn (6.14) corresponds exactly to $\dot{\gamma}_0$ in eqn (6.16). If these factors are set equal to each other, and if the parameters b, μ, B and $\dot{\gamma}_0$ are assumed to be known *a priori*, then the result provides an expression for the dislocation density in terms of these parameters. For example, if $\dot{\gamma}_0=3\times10^7\,\mathrm{s}^{-1}$ is adopted from eqn (5.10) and $B=10^{-5}\,\mathrm{Pa\cdot s}$, $b=3\times10^{-10}\,\mathrm{m}$ and $\mu=7\times10^4\,\mathrm{MPa}$, the implied value of the mobile dislocation density is $N=5\times10^{10}\,\mathrm{m}^{-2}$. This value falls within the range of conceivable results, and is of the same order of magnitude as the dislocation densities observed following fast fracture of single crystals of iron–silicon in Ref. [29] and of tungsten in Ref. [30].

To pursue the correspondence a bit further, the dimensionless factor $\hat{H}(m)$ in eqn (6.14) is compared to $H(m)$ in eqn (6.16) over the full range of crack speed m. The correspondence is shown in Fig. 22 for the case $\omega=45°$. While the two results differ significantly in detail, it is perhaps surprising that the difference in numerical values is no greater in view of the seemingly different assumptions in the two approaches. The implication is that both the continuum plasticity analysis and the simplified dislocation dynamics analysis lead to essentially one and the same conclusion concerning necessary conditions for cleavage crack growth in metals. A number of details of the dislocation modeling could be carried out more realistically. For example, the interaction between dislocations, both on the same glide plane and on nearby planes, has been neglected. As a consequence each dislocation sees the unperturbed stress field associated with K, and this accounts for the factor G^2 in the dissipation term in eqn (6.14) as opposed to G_{tip}^2 in eqn (6.16).

In the previous section the importance of the nondimensional parameter P_c to cleavage cracking was emphasized. If $\zeta=\dot{\gamma}_i\mu/(\dot{\gamma}_0\tau_i)$ is neglected, then from eqn (5.5)

$$P_c=\frac{1}{3}\,\frac{\mu\dot{\gamma}_0 G_{tip}^c}{c_s\tau_i^2}. \qquad (6.17)$$

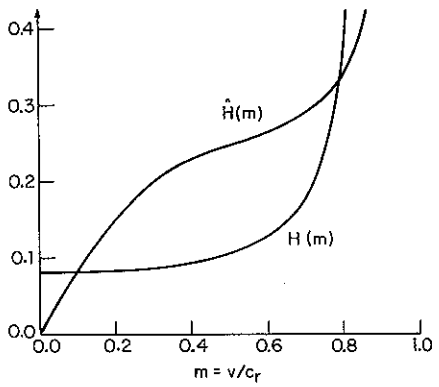

Fig. 22. Comparison of dimensionless factor $H(m)$ derived in continuum analysis to dimensionless factor $\hat{H}(m)$ derived in dislocation analysis for the case $\omega=45°$.

Replacing $\dot{\gamma}_0$ by $(Nb^2\mu/B)$ as motivated above, one can rewrite P_c as

$$P_c = \frac{1}{3}\left(\frac{Nb^3\mu}{Bc_s}\right)\left(\frac{\mu G^c_{tip}}{b\tau_i^2}\right), \qquad (6.18)$$

where each term in brackets is nondimensional. The nondimensional combination $\mu\Gamma/(b\tau_i^2)$, where Γ is the surface energy, was singled out in Ref. [38] as a candidate parameter for separating materials which can potentially cleave from those for which excess crack tip plasticity excludes cleavage. Values of $\mu\Gamma/(b\tau_i^2)$ were tabulated in Ref. [38] for many materials, and the parameter ranged from order unity for non-cleavable metals to order 10^{-4} for easily cleavable substances such as lithium fluoride or ice. The parameter P_c identified by the present analysis involves somewhat more information about the state of the solid. In particular, it depends explicitly on the mobile dislocation density and on the ease of dislocation motion as measured by the drag coefficient B. In addition, the dependence on G^c_{tip}, rather than on just Γ, includes the influence of the fracture morphology.

Acknowledgement—The work of P.A.M. and J.W.H. was supported in part by NSF Grants DMR-83-16979 and MSM-84-16392, and by the Division of Applied Sciences, Harvard University. The work of L.B.F. was supported in part by ONR Contract N00014-85-K-0597 and in part by ARO Contract DAAG29-85-K-0003.

J.W.H. acknowledges discussions with colleagues of the Summer Research Group in Materials Science at the Los Alamos National Laboratory.

REFERENCES

1. Rice J. R. and Thomson R. M., *Phil. Mag.* **29,** 73 (1974).
2. deCelis B., Argon A. S. and Yip S., *J. appl. Phys.* **54,** 4864 (1983).
3. Jokl M. L., Vitek V. and McMahon C. J., *Acta metall.* **28,** 1479 (1980).
4. Ashby M. F. and Embury J. D., *Scripta metall.* **19,** 557 (1985).
5. Stroh A. N., *Advances in Physics* **6,** 418 (1957).
6. Mataga P. A., Ph.D. thesis, Harvard University (1986).
7. Freund L. B. and Hutchinson J. W., *J. Mech. Phys. Solids* **33,** 169 (1985).
8. Freund L. B., Hutchinson J. W. and Lam P. S., *Engng. Frac. Mech.* **23,** 119 (1986).
9. Campbell J. D. and Ferguson W. G., *Phil. Mag.* **21,** 63 (1970).
10. Clifton R. J., *J. appl. Mech.* **50,** 941 (1983).
11. Follansbee P. S., Regazzoni G. and Kocks U. F., *Mechanical Properties at High Rates of Strain* (Edited by J. Harding). Institute of Physics, London (1984).
12. Duffy J., Air Force Wright Aeronautical Laboratories Technical Report AFWAL-TR-82-4024 (1982).
13. Frost H. J. and Ashby M. F., *Deformation Mechanism Maps*. Pergamon Press, Oxford (1982).
14. Freund L. B., *Mechanics Today* (Edited by S. Nemat-Nasser), Vol. III. Pergamon Press, Oxford (1976).
15. Kanninen M. F. and Popelar C. H., *Advanced Fracture Mechanics*. Oxford University Press, Oxford (1985).
16. Hui C. Y. and Riedel H., *Int. J. Fracture* **17,** 409 (1981).
17. Lo K. K., *J. Mech. Phys. Solids* **31,** 287 (1983).
18. Brickstad B., *J. Mech. Phys. Solids* **31,** 307 (1983).
19. Hart E. W., *Int. J. Solids and Structures* **16,** 807 (1980).
20. Chitaley A. D. and McClintock F. A., *J. Mech. Phys. Solids* **19,** 147 (1971).
21. Rice J. R., *Fracture* (Edited by H. Liebowitz), Vol. II. Academic Press, New York (1968).
22. McClintock F. A. and Irwin G. R., *Fracture Toughness Testing and Its Applications*, ASTM STP 381 (1965).
23. Freund L. B. and Douglas A. S., *J. Mech. Phys. Solids* **30,** 59 (1982).
24. Rosakis A. J., Duffy J. and Freund L. B., *J. Mech. Phys. Solids* **32,** 443 (1984).
25. Dean R. and Hutchinson J. W., *12th National Fracture Mechanics Conference*, ASTM STP 700 (1980).
26. Freund L. B. and Douglas A. S., *Elastic-Plastic Fracture*, ASTM STP 803 (Edited by C. F. Shih and J. P. Gudas), Vol. I (1983).
27. Broberg K. B., *High Velocity Deformation of Solids*, IUTAM Symposium, Tokyo, 1977 (Edited by K. Kawata and J. Shioiri). Springer, Berlin (1979).
28. Lin C. and Hoagland R. G., *Fracture Mechanics, Sixteenth Symposium*, ASTM STP 868 (1985).
29. Gerberich W. W. and Kurman E., *Scripta metall.* **19,** 295 (1985).
30. Liu J. M. and Shen B. W., *Metall. Trans. A* **15A,** 1247 (1984).
31. Hahn G. T., *Metall. Trans. A* **1A,** 945 (1984).
32. Kobayashi T., Irwin G. R. and Zhang X.-J., *Fractography of Ceramic and Metal Failures: A Symposium*, ASTM STP 827 (1984).
33. Rosenfield A. R. and Majumdar B. S., "Micromechanics and Toughness for Cleavage of Steel", presented at *International Seminar on Local Approach to Fracture*, Muret-sur-Loing, France (1986).
34. deWitt R. and Fields R., "Measurement of Strains and Strain Rates During Rapid Fracture Events", presented at *Symposium on High Strain Rate Effects in Engineering Materials*, Joint ASCE/ASME Mechanics Conference, Albuquerque (1985).
35. Clark A. B. J. and Irwin G. R., *Exp. Mech.* **6,** 321 (1966).
36. Popelar C. H., "A Visco-Plastic Analysis Predicting the Dynamic Fracture Toughness of A533B Steel", presented at the *19th Nat'l. Symp. on Fracture Mechanics*, June 30–July 2, 1986, San Antonio, Texas.
37. Eshelby J. D., *Phys. Rev.* **90,** 248 (1953).
38. Ashby M. F., unpublished notes on ductile–brittle transition, Summer Research Group, Materials Science Center, Los Alamos National Laboratories (1985).